Biogeochemical protocols and diagnostics for the CMIP6 Ocean Model Intercomparison Project (OMIP)

James C. Orr[1], Raymond G. Najjar[2], Olivier Aumont[3], Laurent Bopp[1], John L. Bullister[4],
Gokhan Danabasoglu[5], Scott C. Doney[6], John P. Dunne[7], Jean-Claude Dutay[1], Heather Graven[8],
Stephen M. Griffies[7], Jasmin G. John[7], Fortunat Joos[9], Ingeborg Levin[10], Keith Lindsay[5],
Richard J. Matear[11], Galen A. McKinley[12], Anne Mouchet[13,14], Andreas Oschlies[15],
Anastasia Romanou[16], Reiner Schlitzer[17], Alessandro Tagliabue[18], Toste Tanhua[15], and Andrew Yool[19]

[1]LSCE/IPSL, Laboratoire des Sciences du Climat et de l'Environnement, CEA-CNRS-UVSQ, Gif-sur-Yvette, France
[2]Dept. of Meteorology, Pennsylvania State University, University Park, Pennsylvania, USA
[3]Laboratoire d'Océanographie et de Climatologie: Expérimentation et Approches Numériques, IPSL, Paris, France
[4]Pacific Marine Environmental Laboratory, NOAA, Seattle, Washington, USA
[5]National Center for Atmospheric Research, Boulder, Colorado, USA
[6]Marine Chemistry & Geochemistry, Woods Hole Oceanographic Institution, USA
[7]NOAA Geophysical Fluid Dynamics Laboratory, Princeton, New Jersey, USA
[8]Dept. of Physics, Imperial College, London, UK
[9]Climate and Environmental Physics, Physics Inst. & Oeschger Center for Climate Change Res., Univ. of Bern, Switzerland
[10]Institut fuer Umweltphysik, Universitaet Heidelberg, Heidelberg, Germany
[11]CSIRO Oceans and Atmosphere, Hobart, Tasmania 7000, Australia
[12]Atmospheric and Oceanic Sciences, University of Wisconsin-Madison, Wisconsin, USA
[13]Max Planck Institute for Meteorology, Hamburg, Germany
[14]Astrophysics, Geophysics and Oceanography Department, University of Liege, Liege, Belgium
[15]GEOMAR Helmholtz Centre for Ocean Research Kiel, Kiel, Germany
[16]Columbia University and NASA-Goddard Institute for Space Studies, New York, NY, USA
[17]Alfred Wegener Institute, Bremerhaven, Germany
[18]Earth, Ocean and Ecological Sciences, University of Liverpool, Liverpool, UK
[19]National Oceanographic Centre, Southampton, UK

Correspondence to: James Orr (james.orr@lsce.ipsl.fr)

Abstract. The Ocean Model Intercomparison Project (OMIP) focuses on the physics and biogeochemistry of the ocean component of Earth System Models participating in the sixth phase of the Coupled Model Intercomparison Project (CMIP6). OMIP aims to provide standard protocols and diagnostics for ocean models, while offering a forum to promote their common assessment and improvement. It also offers to compare solutions of the same ocean models when forced with reanalysis data (OMIP

5   simulations) versus when integrated within fully coupled Earth System Models (CMIP6). Here we detail simulation protocols and diagnostics for OMIP's biogeochemical and inert chemical tracers. These passive-tracer simulations will be coupled online to ocean circulation models, initialized with observational data or output from a model spin up, and forced by repeating the 1948-2009 surface fluxes of heat, fresh water, and momentum. These so-called OMIP-BGC simulations include three inert chemical tracers (CFC-11, CFC-12, SF_6) and biogeochemical tracers (e.g. dissolved inorganic carbon, carbon isotopes, alka-

10   linity, nutrients, and oxygen). Modelers will use their preferred prognostic BGC model but should follow common guidelines for gas exchange and carbonate chemistry. Simulations include both natural and total carbon tracers. The required forced simu-

lation *(omip1)* will be initialized with gridded observational climatologies. An optional forced simulation *(omip1-spunup)* will be initialized instead with BGC fields from a long model spin up, preferably for 2000 years or more and forced by repeating the same 62-year meteorological forcing. That optional run will also include abiotic tracers of total dissolved inorganic carbon and radiocarbon, $C_{\mathrm{T}}^{\mathrm{abio}}$ and $^{14}C_{\mathrm{T}}^{\mathrm{abio}}$, to assess deep-ocean ventilation and distinguish the role of physics vs. biology. These simula-

5 tions will be forced by observed atmospheric histories of the three inert gases and CO_2 as well as carbon isotope ratios of CO_2. OMIP-BGC simulation protocols are founded on those from previous phases of the Ocean Carbon-Cycle Model Intercomparison Project. They have been merged and updated to reflect improvements concerning gas exchange, carbonate chemistry, and new data for initial conditions and atmospheric gas histories. Code is provided to facilitate their implementation.

1 Introduction

10 Centralized efforts to compare numerical models with one another and with data commonly lead to model improvements and accelerated development. The fundamental need for model comparison is fully embraced in Phase 6 of the Coupled Model Intercomparison Project (CMIP6), an initiative that aims to compare Earth System Models and their climate-model counterparts as well as their individual components. CMIP6 emphasizes common forcing and diagnostics through 21 dedicated Model Intercomparison Projects (MIPs) under a common umbrella (Eyring et al., 2016). One of these MIPs is the Ocean Model

15 Intercomparison Project (OMIP). OMIP focuses on comparison of global ocean models that couple circulation, sea-ice, and optional biogeochemistry, which together make up the ocean components of the Earth System Models used within CMIP6. OMIP works along two coordinated branches focused on ocean circulation and sea ice (OMIP-Physics) and on biogeochemistry (OMIP-BGC). The former is described in a companion paper in this same issue (Griffies et al., 2016), while the latter is described here.

20 Groups that participate in OMIP will use different ocean biogeochemical models coupled to different ocean general circulation models (OGCMs). The skill of the latter in simulating ocean circulation affects the ability of the former to simulate ocean biogeochemistry. Thus previous efforts to compare global-scale, ocean biogeochemical models have also strived to evaluate model-predicted patterns of ocean circulation. For instance, the Ocean Carbon-Cycle Model Intercomparison Project (OCMIP) included efforts to assess simulated circulation along with simulated biogeochemistry. OCMIP began in 1995 as an effort to

25 identify the principal differences between existing ocean carbon-cycle models. Its first phase (OCMIP1) included four models and focused on natural and anthropogenic components of oceanic carbon and radiocarbon (Sarmiento et al., 2000; Orr et al., 2001). OCMIP2 was launched in 1998, comparing 12 models with common biogeochemistry, and evaluating them with physical and inert chemical tracers (Doney et al., 2004; Dutay et al., 2002; Matsumoto et al., 2004; Dutay et al., 2004; Orr et al., 2005; Najjar et al., 2007). In 2002, OCMIP3 turned its attention to evaluating simulated interannual variability in forced ocean

30 biogeochemical models (e.g. Rodgers et al., 2004; Raynaud et al., 2006). More recently, OCMIP has focused on assessing ocean biogeochemistry simulated by Earth System Models (e.g. Bopp et al., 2013).

OCMIP2 evaluated simulated circulation using the physically active tracers, temperature T and salinity S (Doney et al., 2004), but also with passive tracers, i.e. those having no effect on ocean circulation. For example, OCMIP2 used two an-

thropogenic transient tracers, CFC-11 and CFC-12 (Dutay et al., 2002). Although these are reactive gases in the atmosphere that participate in the destruction of ozone, they remain inert once absorbed by the ocean. From an oceanographic perspective, they may be thought of as dye tracers given their inert nature and purely anthropogenic origin, increasing only since the 1930s (Fig. 1). Furthermore, precise measurements of CFC-11 and CFC-12 have been made throughout the world ocean, e.g.

5 having been collected extensively during WOCE (World Ocean Circulation Experiment) and CLIVAR (Climate and Ocean—Variability, Predictability and Change). Hence they are well suited for model evaluation and are particularly powerful when used together to deduce decadal ventilation times of subsurface waters. Yet their combination is less useful to assess more recent ventilation, because their atmospheric concentrations have peaked and declined, since 1990 for CFC-11 and since 2000 for CFC-12, as a result of the Montreal Protocol. To fill this recent gap, oceanographers now also measure SF_6, another an-

10 thropogenic, inert chemical tracer whose atmospheric concentration has increased nearly linearly since the 1980s. Combining SF_6 with either CFC-11 or CFC-12 is optimal for assessing even the most recent ventilation time scales. Together these inert chemical tracers can be used to assess transient time distributions (TTDs). TTDs are used to infer distributions of other passive tracer distributions, such as anthropogenic carbon (e.g. Waugh et al., 2003), which cannot be measured directly.

  To help assess simulated circulation fields, OCMIP also included another passive tracer, radiocarbon, focusing on both its

15 natural and anthropogenic components. Radiocarbon (^{14}C) is produced naturally by cosmogenic radiation in the atmosphere, invades the ocean via air-sea gas exchange, and is mixed into the deep sea. Its natural component is useful because its horizontal and vertical gradients in the deep ocean result not only from ocean transport but also from radioactive decay (half-life of 5700 years), leaving a time signature for the slow ventilation of the deep ocean (roughly 100 to 1000 yr depending on location). Hence natural ^{14}C provides rate information throughout the deep ocean, unlike T and S. For example, the ventilation age

20 of the deep North Pacific is about 1000 years, based on the depletion of its $^{14}C/C$ ratio (-260‰ in terms of $\Delta^{14}C$, i.e. the fractionation-corrected ratio relative to that of the preindustrial atmosphere) when compared with that of source waters from the surface Southern Ocean (-160‰) (Toggweiler et al., 1989a). The natural component of radiocarbon complements the three inert chemical tracers mentioned above, which are used to assess more recently ventilated waters nearer to the surface. Yet the natural component is only half of the story.

25 During the industrial era, atmospheric $\Delta^{14}C$ declined due to emissions of fossil CO_2 (Suess effect) until the 1950s when that signal was overwhelmed by the much larger spike from atmospheric nuclear weapons tests (Fig. 2). Since the latter dominates, the total change from both anthropogenic effects is often referred to as bomb radiocarbon. As an anthropogenic transient tracer, bomb radiocarbon complements CFC-11, CFC-12, and SF_6 because of its different atmospheric history and much longer air-sea equilibration time (Broecker and Peng, 1974). Observations of bomb radiocarbon have been used to constrain the global

30 mean gas transfer velocity (Broecker and Peng, 1982; Sweeney et al., 2007); however, in recent decades, ocean radiocarbon changes have become more sensitive to interior transport and mixing, making it behave more like anthropogenic CO_2 (Graven et al., 2012). Hence it is particularly relevant to use radiocarbon observations to evaluate ocean carbon-cycle models that aim to assess uptake of anthropogenic carbon as done during OCMIP (e.g. Orr et al., 2001).

  Information from the stable carbon isotope ^{13}C also helps to constrain the anthropogenic perturbation in dissolved inorganic

35 carbon by exploiting the Suess effect (Quay et al., 1992, 2003). Driven by the release of anthropogenic CO_2 produced from

providing fundamental information necessary to improve near-term climate prediction and carbon feedbacks in the climate system.

2   Protocols

As described by Griffies et al. (2016), the OMIP-Physics simulations consist of forcing physical model systems (an ocean
5   general circulation model coupled to a sea-ice model) with the interannually varying atmospheric data reanalysis known as the Coordinated Ocean-ice Reference Experiments (CORE-II) available over 1948 to 2009 (Large and Yeager, 2009). For OMIP, that 62-yr forcing will be repeated five times to make simulations of 310 yr. OMIP-BGC participants will make these simulations by coupling their prognostic models of ocean biogeochemistry, online, to their physical model systems. These OMIP-BGC simulations will be forced by observed records of atmospheric CO_2 and other gases during the 310-yr period,
10   defined as equivalent to calendar years 1700 to 2009. One 310-yr OMIP simulation *(omip1)*, with models initialized by data, is required (Tier 1) for all OMIP modeling groups; another 310-yr simulation *(omip1-spunup)*, with models initialized from a previous long spin-up simulation, is only for OMIP-BGC groups. Although optional, the *omip1-spunup* simulation is strongly encouraged (Tier 2) to minimize drift, assess deep-ocean ventilation, and separate physical vs. biological components of ocean carbon. Details of these simulations are provided below.

15   When modeling chemical and biogeochemical tracers, it is recommended that OMIP groups use the same formulations for gas exchange and carbonate chemistry as outlined below. Little effort would be needed to modify code that is already consistent with previous phases of OCMIP. For gas exchange, model groups only need to change the value of the gas transfer coefficient, the formulations and coefficients for Schmidt numbers, and the atmospheric gas histories. For carbonate chemistry, groups should strive to use the constants recommended for best practices (Dickson et al., 2007) on the total pH scale and to avoid
20   common modeling assumptions that lead to significant biases, notably an oversimplified alkalinity equation (Orr and Epitalon, 2015). Fortran 95 code to make these calculations will be made available to OMIP-BGC participants.

2.1   Passive Tracers

2.1.1   Inert chemistry

The inert chemistry component of OMIP includes online simulation of CFC-11, CFC-12, and SF_6. While CFC-12 is required
25   (level=1), CFC-11 and SF_6 are encouraged (level=2). About the same amount of observational data in the global ocean exists for both CFC-11 and CFC-12, starting with early field programs in the 1980s. But CFC-12 has a longer atmospheric history, with its production starting a decade earlier (∼1936) and a slower decline starting a decade later due to its longer atmospheric lifetime (112 vs. 52 yr) relative to CFC-11 (Rigby et al., 2013). In contrast, SF_6 has continued to increase rapidly in recent decades. That increase will continue for many years despite ongoing efforts to restrict production and release of this potent
30   greenhouse gas, because SF_6's atmospheric lifetime is perhaps 3000 yr (Montzka et al., 2003). Using pairs of these tracers

offers a powerful means to constrain ventilation ages; if model groups are only able to model two of these tracers, the ideal combination is CFC-12 and SF_6.

Simulation protocols are based on the OCMIP2 design document (Najjar and Orr, 1998) and its ensuing CFC protocol (Orr et al., 1999a) and model comparison (Dutay et al., 2002). These inert passive tracers are computed online along with the

5   active tracers (i.e. temperature and salinity in the physical simulation); they are independent of the biogeochemical model. OMIP models will be forced to follow historical atmospheric concentrations of CFC-11, CFC-12, and SF_6, accounting for gas exchange and their different solubilities and Schmidt numbers. The same passive tracers should be included in the forced OMIP simulations and in the coupled CMIP6 historical simulations. Both types of simulations will be analyzed within the framework of OMIP. These inert chemistry tracers are complementary to the ideal age tracer that is included in the OMIP-Physics protocols

10   (Griffies et al., 2016).

2.1.2 Biogeochemistry

For the other passive tracers, referred to as biogeochemistry, the OMIP-BGC protocols build on those developed for OCMIP. These include the OCMIP2 abiotic and biotic protocols (Najjar and Orr, 1998, 1999; Orr et al., 1999b) and the OCMIP3 protocols for interannually forced simulations (Aumont et al., 2004). Each model group will implement the OMIP protocol

15   in their own prognostic ocean biogeochemical model as in OCMIP3, unlike the common-model approach of OCMIP2. Each OMIP biogeochemical model will be coupled online to an ocean general circulation model, forced by the CORE-II atmospheric state. Geochemical boundary conditions for the atmosphere include an imposed constant atmospheric concentration of O_2 (mole fraction x_{O_2} of 0.20946) but a variable atmospheric CO_2 that follows observations (Meinshausen et al., 2016).

In addition, OMIP-BGC simulations will require a natural carbon tracer that sees a constant atmospheric mole fraction of

20   CO_2 in dry air (x_{CO_2}) fixed at the 1 January 1850 value (284.65 ppm), the CMIP6 preindustrial reference. This can be done either in an independent simulation with identical initial conditions and forcing, except for atmospheric x_{CO_2}, or in the same simulation by adding one or more new tracers to the biogeochemical model, referred to here as a *dual-C_T* simulation. For this *dual* simulation, OMIP modelers would need to add a second dissolved inorganic carbon tracer (C_T^{nat}), e.g. as in Yool et al. (2010). In OMIP, this added tracer will isolate natural CO_2 and keep track of model drift. Such *doubling* may also be

25   necessary for other biogeochemical model tracers if they are directly affected by the CO_2 increase. For instance, expansion of the PISCES model (Aumont and Bopp, 2006) to a *dual-C_T* implementation resulted in doubling not only C_T but also its transported $CaCO_3$ tracer, which in turn affects total alkalinity A_T (Dufour et al., 2013). These natural tracers are referred to as C_T^{nat}, $CaCO_3^{nat}$, and A_T^{nat}. Calculated variables affected by CO_2 should also be doubled, including pH, pCO_2, the air-sea CO_2 flux, and carbonate ion concentration. If biology depends on CO_2, additional tracers such as nutrients and O_2 would also need

30   to be doubled, making the doubling strategy less appealing. That strategy may also be more complex in some Earth System Models, e.g. if A_T changes abiotically due to warming-related changes in weathering and river runoff.

2.1.3 Abiotic carbon and radiocarbon

In the *omip1-spunup* simulation (as well as in its previously run spin up) OMIP-BGC groups will also include two abiotic tracers to simulate total dissolved inorganic carbon C_T^{abio} and corresponding radiocarbon $^{14}C_T^{abio}$. These abiotic tracers do not depend on any biotic tracers. They should be included in addition to the biotic carbon tracers mentioned above (C_T and C_T^{nat}).

5   The ratio of the two abiotic tracers will be used to evaluate and compare models in terms of deep-ocean ventilation ages (natural radiocarbon) and near-surface anthropogenic invasion of bomb radiocarbon. In addition, C_T^{abio} will be compared to C_T to distinguish physical from biogeochemical effects on total carbon. For simplicity, simulations will be made abiotically following OCMIP2 protocols (Orr et al., 1999b). We recommend that participating groups add these two independent tracers to their biogeochemical model to simulate them simultaneously, thus promoting internal consistency while reducing costs.

10   In OMIP, we will use this two-tracer approach rather than the simpler approach of modeling only the ^{14}C/C ratio directly (Toggweiler et al., 1989a, b). That simpler approach would be a better choice if our focus were only on comparing simulated and field-based estimates of the ocean's bomb-^{14}C inventory, both of which are biased low (Naegler, 2009; Mouchet, 2013). The simpler modeling approach underestimates the inventory, because it assumes a constant air-sea CO_2 disequilibrium during the industrial era; likewise, field reconstructions of the ocean's bomb-^{14}C inventory (Key et al., 2004; Peacock, 2004; Sweeney

15 et al., 2007) are biased low because they assume that ocean C_T is unaffected by the anthropogenic perturbation. Yet in terms of oceanic Δ^{14}C, the simple and the two-tracer approaches yield similar results (Mouchet, 2013), because the effect of increasing C_T on oceanic Δ^{14}C is negligible (Naegler, 2009). We also choose the two-tracer approach to take advantage of its C_T^{abio} tracer to help distinguish physical from biological contributions to C_T.

  To model ^{14}C, OMIP neglects effects due to fractionation (i.e. from biology and gas exchange). Hence model results will

20 be directly comparable to measurements reported as Δ^{14}C, a transformation of the ^{14}C/C ratio designed to correct for fractionation (Toggweiler et al., 1989a). Thus biases associated with our abiotic approach may generally be neglected. For natural ^{14}C, Bacastow and Maier-Reimer (1990) found essentially identical results for simulations that accounted for biological fractionation vs. those that did not, as long as the atmospheric CO_2 boundary conditions were identical. For bomb ^{14}C, which also includes the Suess effect, neglecting biological fractionation results in small biases (Joos et al., 1997).

25   Hence for the *omip1-spunup* simulation, OMIP-BGC groups will simulate four flavors of dissolved inorganic carbon: biotic natural (C_T^{nat}), biotic total (C_T), abiotic total (C_T^{abio}), and abiotic radiocarbon ($^{14}C_T^{abio}$). Conversely for the *omip1* simulation, groups will simulate only the first two flavors, C_T^{nat} and C_T. These tracers may be simulated simultaneously or in separate simulations, although we recommend the former.

2.1.4 Carbon-13

30 Modeling groups that will simulate ocean ^{13}C are requested to report net air-sea fluxes of $^{13}CO_2$ and concentrations of total dissolved inorganic carbon-13 ($^{13}C_T$) for the *omip1-spunup* simulation. In Sect. 2.5 we recommend how isotopic fractionation during gas exchange should be modeled. Carbon-13 is typically included in ocean models as a biotic variable influenced by fractionation effects during photosynthesis that depend on growth rate and phytoplankton type. Some models also include

fractionation during calcium carbonate formation. Modeling groups should incorporate ecosystem fractionation specific to their ecosystem model formulation. We do not request modeling groups to report variables related to ^{13}C in phytoplankton or other organic carbon pools, only ^{13}C$_T$ and net air-sea ^{13}CO$_2$ fluxes.

2.2 Duration and initialization

5 As described by (Griffies et al., 2016), the physical components of the models are to be forced over 310 years, i.e. over five repeated forcing cycles of the 62-year CORE-II forcing (1948–2009). The biogeochemistry should be included, along with the physical system, during the full 310 years (1700–2009) and the inert chemistry only during the last 74 years (1936–2009). The biogeochemical simulations will be initialized on calendar date 01 January 1700, at the start of the first CORE-II forcing cycle. The inert anthropogenic chemical tracers (CFC-11, CFC-12, SF$_6$) will be initialized to zero on 01 January 1936, during the
10 fourth CORE-II forcing cycle at model date 01 January 0237.

For the *omip1* simulation, biogeochemical tracers will be initialized generally with observational climatologies. Fields from the 2013 World Ocean Atlas (WOA2013) will be used to initialize model fields of oxygen (Garcia et al., 2014a) as well as nitrate, total dissolved inorganic phosphorus, and total dissolved inorganic silicon (Garcia et al., 2014b). The latter two nutrients are often referred to simply as phosphate and silicate, but other inorganic P and Si species also contribute substantially to each
15 total concentration (Fig. 3). Indeed it is the total dissolved concentrations (P_T and Si_T) that are both modeled and measured. OMIP will provide all these initial biogeochemical fields by merging WOA2013's means for January, available down to 500 m (for nitrate, phosphate and silicate), and down to 1500m for oxygen, with its annual mean fields below.

Model fields for A_T and preindustrial C_T will be initialized with gridded data from version 2 of the Global Ocean Data Analysis Project (GLODAPv2) from Lauvset et al. (2016), based on discrete measurements during WOCE and CLIVAR
20 (Olsen et al., 2016). To initialize modeled dissolved organic carbon (DOC), OMIP provides fields from the adjoint model from Schlitzer (Hansell et al., 2009). For dissolved iron (Fe), OMIP simulations will not be initialized from observations because a full-depth, global 3-D data climatology is unavailable due to lack of data coverage, particularly in the deep ocean. Hence for initial Fe fields, OMIP provides the median model result from the Iron Model Intercomparison Project (FeMIP, Tagliabue et al., 2016). Yet that initialization field may not be well suited for all Fe models, which differ greatly. Although
25 OMIP provides initialization fields for Fe and DOC, their actual initialization is left to the discretion of each modeling group. In a previous comparison (Kwiatkowski et al., 2014), groups did not initialize modeled Fe with a common field nor approach because the complexity of the Fe cycle differed greatly among models. Likewise, there was no common approach to initialize DOC because biogeochemical models vary greatly in the way they represent its lability. Initialization of other tracers is less critical, e.g. phytoplankton biomass is restricted to the top 200 m and equilibrates rapidly as do other biological tracers.

30 The *omip1* simulation is relatively short and is thus manageable by all groups, but many of its tracers will have large drifts because model initial states will be far from their equilibrium states. These drifts complicate assessment of model performance based on model-data agreement (Séférian et al., 2015). Hence a complementary simulation, *omip1-spunup*, is proposed, where biogeochemical tracers are initialized instead with a near-equilibrium state. Model groups may generate this spun-up initial state by any means at their disposal. The classic approach would be to spin up the model. That could be done either online,

repeating many times the same physical atmospheric forcing (CORE-II), or offline, repeatedly cycling the physical transport fields from a circulation model forced by a single loop of the CORE-II forcing. If possible, the spin-up should be run until it reaches the equilibrium criteria adopted for OCMIP2. These criteria state that the globally integrated, biotic and abiotic air-sea CO_2 fluxes (F_{CO_2} and $F_{CO_2}^{abio}$) should each drift by less than $0.01\,\mathrm{Pg\,C\,yr^{-1}}$ (Najjar and Orr, 1999; Orr et al., 1999b) and that

5 abiotic $^{14}C_T$ should be stabilized to the point that 98% of the ocean volume has a drift of less than $0.001\,\text{‰}\,\mathrm{yr^{-1}}$ (Aumont et al., 1998). The latter is equivalent to a drift of about 10 yr in the ^{14}C age per 1000 yr of simulation. For most models, these drift criteria can be reached only after integrations of a few thousand model years. To reach the spun-up state with the classic approach, we request that groups spin up their model for at least 2000 yr, if at all possible. Other approaches to obtain the spun-up state, such as using tracer-acceleration techniques or fast solvers (Li and Primeau, 2008; Khatiwala, 2008; Merlis and

10 Khatiwala, 2008) are also permissible. If used, they should also be applied until models meet the same equilibrium criteria described above.

The spin-up simulation itself should be initialized as for the *omip1* simulation, except for the abiotic tracers and the $^{13}C_T$ tracer. The abiotic initial fields of A_T^{abio} and C_T^{abio} will be provided, being derived from initial fields of T and S. Although C_T^{abio} is a passive tracer carried in the model, A_T^{abio} is not. The latter will be calculated from the initial 3-D salinity field as

15 detailed below; then that calculated field will be used to compute C_T^{abio} throughout the water column assuming equilibrium with the preindustrial level of atmospheric CO_2 at the initial T and S conditions (using OMIP's carbonate chemistry routines). For $^{14}C_T^{abio}$, initial fields will be based on those from GLODAPv1 for natural $\Delta^{14}C$ (Key et al., 2004). OMIP will provide these fields with missing grid <cells filled based on values from adjacent ocean grid points. Groups that include $^{13}C_T$ in *omip1-spunup* should initialize that in the precursor spin-up simulation to 0‰ following the approach of Jahn et al. (2015). Beware

20 though that equilibration timescales for ^{13}C are longer than for C_T, implying the need for a much longer spin up.

2.3 Geochemical atmospheric forcing

The atmospheric concentration histories of the three inert chemical tracers (CFC-11, CFC-12, and SF_6) to be used in OMIP are summarized by Bullister (2015) and shown in Fig. 1. Their atmospheric values are to be held to zero for the first three cycles of the CORE-II forcing, then increased starting on 01 January 1936 (beginning of model year 0237) according to the OMIP

25 protocol. To save computational resources, the inert chemical tracers may be activated only from 1936 onward, starting from zero concentrations in the atmosphere and ocean. The atmospheric CO_2 history used to force the OMIP models is the same as that used for the CMIP6 historical simulation (Meinshausen et al., 2016), while carbon isotope ratios ($\Delta^{14}C$ and $\delta^{13}C$) are the same as those used by C4MIP (Jones et al., 2016). These atmospheric records of CO_2 and carbon isotope ratios (Fig. 2) and those for the inert chemical tracers will be made available on the CMIP6 web site. The biogeochemical tracers are to be

30 activated at the beginning of the 310-year simulation (on 01 January 1700), but initialized differently as described above for *omip1* and *omip1-spunup*. The atmospheric concentration of CO_2 is to be maintained at the CMIP6 preindustrial reference of $xCO_2^{atm} = 284.65$ ppm between calendar years 1700.0 and 1850.0, after which it must increase following observations (Meinshausen et al., 2016). The increasing xCO_2^{atm} will thus affect C_T but not C_T^{nat}, which sees only the preindustrial reference

level of $x\mathrm{CO}_2^{\mathrm{atm}}$. The increasing $x\mathrm{CO}_2^{\mathrm{atm}}$ is also seen by $^{13}C_{\mathrm{T}}$ and the two abiotic tracers, C_{T}^{abio} and $^{14}C_{\mathrm{T}}^{\mathrm{abio}}$, to be modeled only in the *omip1-spunup* simulation and its spin up.

2.4 Conservation equation

The time evolution equation for all passive tracers is given by

$$\frac{\partial C}{\partial t} = \mathbf{L}(C) + J_C,$$ (1)

where C is the tracer concentration; $\mathbf{L}$ is the 3-D transport operator, which represents effects due to advection, diffusion, and convection; and J_C is the internal source-sink term. Conservation of volume is assumed in Eq. 1 and standard units of $\mathrm{mol\,m^{-3}}$ are used for all tracers. For the inert chemical tracers (CFC-11, CFC-12, and SF_6), $J_C = 0$. For the abiotic carbon tracers, in the *omip1-spunup* simulation and its spin up, the same term is also null for the total carbon tracer C_{T}

$$J_{C_{\mathrm{T}}^{\mathrm{abio}}} = 0,$$ (2)

but not for the total radiocarbon tracer $^{14}C_{\mathrm{T}}^{\mathrm{abio}}$ due to radioactive decay

$$J_{^{14}C_{\mathrm{T}}^{\mathrm{abio}}} = -\lambda \, ^{14}C_{\mathrm{T}}^{\mathrm{abio}},$$ (3)

where λ is the radioactive decay constant for $^{14}\mathrm{C}$, i.e.

$$\lambda = ln(2)/5700\,\mathrm{yr} = 1.2160 \times 10^{-4}\,\mathrm{yr^{-1}},$$ (4)

converted to $\mathrm{s^{-1}}$ using the number of seconds per year in a given model. For other biogeochemical tracers J_C is non-zero and often differs between models. For $^{13}C_{\mathrm{T}}$, J_C includes isotopic fractionation effects.

2.5 Air-sea gas exchange

Non-zero surface boundary conditions must also be included for all tracers that are affected by air-sea gas exchange: CFC-11, CFC-12, SF_6, dissolved O_2, and dissolved inorganic carbon in its various modeled forms (C_{T}, $C_{\mathrm{T}}^{\mathrm{nat}}$, $C_{\mathrm{T}}^{\mathrm{abio}}$, $^{14}C_{\mathrm{T}}^{\mathrm{abio}}$, and $^{13}C_{\mathrm{T}}$). In OCMIP2, surface boundary conditions also included a virtual-flux term for some biogeochemical tracers, namely in models that had a virtual salt flux because they did not allow water transfer across the air-sea interface. Water transfer calls for different implementations depending on the way the free-surface is treated, as discussed extensively by Roullet and Madec (2000). Groups that have implemented virtual fluxes for active tracers (T and S) should follow the same practices to deal with virtual fluxes of passive tracers such as C_{T} and A_{T}, as detailed in the OCMIP2 design document (Najjar and Orr, 1998) and in the OCMIP2 Abiotic HOWTO (Orr et al., 1999b). In OMIP, all models should report air-sea CO_2 fluxes due to gas exchange (F_{CO_2}, $F_{\mathrm{CO}_2}^{\mathrm{nat}}$, $F_{\mathrm{CO}_2}^{\mathrm{abio}}$, $F_{^{14}\mathrm{CO}_2}^{\mathrm{abio}}$, and $F_{^{13}\mathrm{CO}_2}$) without virtual fluxes included. Virtual fluxes are not requested as they do not directly represent CO_2 exchange between the atmosphere and ocean.

Surface boundary fluxes may be coded simply as adding source-sink terms to the surface layer, e.g.

$$J_A = \frac{F_A}{\Delta z_1},$$ (5)

where for gas A, J_A is its surface-layer source-sink term due to gas exchange ($\mathrm{mol\,m^{-3}\,s^{-1}}$) and F_A is its air-to-sea flux ($\mathrm{mol\,m^{-2}\,s^{-1}}$), while Δz_1 is the surface-layer thickness (m).

In OMIP, we parameterize air-sea gas transfer of CFC-11, CFC-12, SF_6, O_2, CO_2, $^{14}CO_2$, and $^{13}CO_2$ using the gas transfer formulation also adopted for OCMIP2 (excluding effects of bubbles):

$$F_A = k_w \left([A]_{sat} - [A]\right), \tag{6}$$

where for gas A, k_w is its gas transfer velocity, $[A]$ is its simulated surface-ocean dissolved concentration, and $[A]_{sat}$ is its corresponding saturation concentration in equilibrium with the water-vapor-saturated atmosphere at a total atmospheric pressure P_a. Concentrations throughout are indicated by square brackets and are in units of $\mathrm{mol\,m^{-3}}$.

For all gases that remain purely in dissolved form in seawater, gas exchange is modeled directly with Eq. (6). However for C_{T}, only a small part remains as dissolved gas as mentioned in Sect. 2.6. Thus the dissolved gas concentration $[CO_2^*]$ must first be computed, each time step, from modeled C_{T} and A_{T} and then the gas exchange is computed with Eq. (6). For example, for the two abiotic tracers (in *omip1-spunup*):

$$F_{CO_2}^{\mathrm{abio}} = k_w \left([CO_2^*]_{sat} - [CO_2^*]\right) \tag{7}$$

and

$$F_{^{14}CO_2}^{\mathrm{abio}} = k_w \left(\left[^{14}CO_2^*\right]_{sat} - \left[^{14}CO_2^*\right]\right). \tag{8}$$

For ^{13}C, isotopic fractionation associated with gas exchange must be included in the flux calculation. We recommend using the formulation of Zhang et al. (1995)

$$F_{^{13}CO_2} = k_w\,\alpha_k\,\alpha_{aq-g}\left(^{13}R_{\mathrm{atm}}\,[CO_2^*]_{\mathrm{sat}} - \frac{\left[^{13}CO_2^*\right]}{\alpha_{C_{\mathrm{T}}-g}}\right), \tag{9}$$

where α_k is the kinetic fractionation factor, α_{aq-g} is the fractionation factor for gas dissolution, and $\alpha_{C_{\mathrm{T}}-g}$ is the equilibrium fractionation factor between dissolved inorganic carbon and gaseous CO_2. $^{13}R_{\mathrm{atm}}$ is the $^{13}C/^{12}C$ ratio in atmospheric CO_2. Following Zhang et al. (1995), $\alpha_{C_{\mathrm{T}}-g}$ depends on T and the fraction of carbonate in C_T, fCO_3:

$$\alpha_{C_{\mathrm{T}}-g} = \frac{0.0144\,T_c\,fCO_3 - 0.107\,T_c + 10.53}{1000} + 1, \tag{10}$$

where T_c is temperature in units of °C, while division by 1000 and addition of 1 converts the fractionation factor from ϵ in units of ‰ into α. The α_{aq-g} term depends on temperature following

$$\alpha_{aq-g} = \frac{0.0049\,T_c - 1.31}{1000} + 1. \tag{11}$$

Conversely no temperature dependence was found for α_k. Hence we recommend that OMIP modelers use a constant value for α_k of 0.99914 (ϵ_k of -0.86‰), the average from Zhang et al.'s measurements at 5° and 21°C.

2.5.1 Gas transfer velocity

OMIP modelers should use the instantaneous gas transfer velocity k_w parameterization from Wanninkhof (1992), a quadratic function of the 10-m wind speed u

$$k_W = a \left(\frac{Sc}{660} \right)^{-1/2} u^2 \left(1 - f_i\right), \tag{12}$$

5   to which we have added limitation from sea-ice cover following OCMIP2. Here a is a constant, Sc is the Schmidt number, and f_i is the sea-ice fractional coverage of each grid cell (varying from 0 to 1). Normally, the constant a is adjusted so that wind speeds used to force the model are consistent with the observed global inventory of bomb ^{14}C, e.g. as done in previous phases of OCMIP (Orr et al., 2001; Najjar et al., 2007). Here though, we choose to use one value of a for all simulations, independent of whether models are used in forced (OMIP) or coupled mode (i.e. in CMIP6 DECK [Diagnostic, Evaluation and

10   Characterization of Klima] and historical simulations). For a in OMIP, we rely on the reassessment from Wanninkhof (2014) who used improved estimates of the global-ocean bomb-^{14}C inventory along with CCMP (Cross Calibrated Multi-Platform) wind fields in an inverse approach with the Modular Ocean Model (Sweeney et al., 2007) to derive a best value of

$$a = 0.251 \, \frac{\mathrm{cm\,hr^{-1}}}{(\mathrm{m\,s^{-1}})^2}, \tag{13}$$

which will give k_w is in $\mathrm{cm\,hr^{-1}}$ if winds speeds are in $\mathrm{m\,s^{-1}}$. For model simulations where tracers are carried in $\mathrm{mol\,m^{-3}}$, k_w

15   should be in units of $\mathrm{m\,s^{-1}}$; thus, a should be set equal to $6.97 \times 10^{-7}\,\mathrm{m\,s^{-1}}$. The same value of a should be adopted for the forced OMIP simulations and for Earth System Model simulations made under CMIP6.

2.5.2 Schmidt number

Besides a, the Schmidt number Sc is also needed to compute the gas transfer velocity (Eq. 12). The Schmidt number is the ratio of the kinematic viscosity of water μ to the diffusion coefficient of the gas D ($Sc = \mu/D$). The coefficients for the fourth-order

20   polynomical fit of Sc to *in situ* temperature over the temperature range of -2 to $40°$C (Wanninkhof, 2014) are provided in Table 1 for each gas to be modeled in OMIP and CMIP6. Fortran 95 routines using the same formula and coefficients for all gases modeled in OMIP are available for download via the *gasx* module of the *mocsy* package (Sect. 2.6).

2.5.3 Atmospheric saturation concentration

The surface gas concentration in equilibrium with the atmosphere (saturation concentration) is

$$[A]_{sat} = K_0 \, f_A = K_0 \, C_f \, p_A = K_0 \, C_f \, (P_a - p\mathrm{H_2O}) \, x_A, \tag{14}$$

where for gas A, K_0 is its solubility, f_A is its atmospheric fugacity, C_f is its fugacity coefficient, p_A is its atmospheric partial pressure, and x_A is its mole fraction in dry air, while P_a is again the total atmospheric pressure (atm) and $p\mathrm{H_2O}$ is the water vapor pressure at saturation (also in atm) (Weiss and Price, 1980).

The combined term $K_0 C_f (P_a - pH_2O)$ is available at $P_a = 1$ atm (i.e. P_a^0) for all modeled gases except oxygen. We denote this combined term as ϕ_A^0 (at P_a^0) ; elsewhere it is known as the solubility function F (e.g. Weiss and Price, 1980; Warner and Weiss, 1985; Bullister et al., 2002) but we do not use the latter notation here to avoid confusion with the air-sea flux (Eq. 6). For four of the gases to be modeled in OMIP, the combined solubility function ϕ_A^0 has been computed using the empirical fit

$$5 \quad ln\left(\phi_A^0\right) = a_1 + a_2 \left(\frac{100}{T}\right) + a_3 \, ln\left(\frac{T}{100}\right) + a_4 \left(\frac{T}{100}\right)^2 + S\left[b_1 + b_2\left(\frac{T}{100}\right) + b_3\left(\frac{T}{100}\right)^2\right], \quad (15)$$

where T is the model's in-situ, absolute temperature and S is its salinity in permil. Thus separate sets of coefficients are available for CO_2 (Weiss and Price, 1980, Table VI), CFC-11 and CFC-12 (Warner and Weiss, 1985, Table 5), and SF_6 (Bullister et al., 2002, Table 3), the values of which are detailed in Table 2. For O_2, it is not ϕ_A^0 that is available but rather $[O_2]_{sat}^0$ (Garcia and Gordon, 1992) as detailed below.

10   Both the solubility function ϕ_A^0 and the saturation concentration $[A]_{sat}^0$ can be used at any atmospheric pressure P_a, with errors of less than 0.1%, by approximating Eq. (14) as

$$[A]_{sat} = \frac{P_a}{P_a^0} \, \phi_A^0 \, x_A = \frac{P_a}{P_a^0} \, [A]_{sat}^0, \quad (16)$$

where P_a^0 is the reference atmospheric pressure (1 atm). Variations in surface atmospheric pressure must not be neglected in OMIP because they alter the regional distribution of $[A]_{sat}$. For example, the average surface atmospheric pressure between
15   $60°$ and $30°$S is 3% lower than the global mean, thus reducing surface-ocean pCO_2 by $10\,\mu$atm and $[O_2]_{sat}$ by $10\,\mu$mol kg^{-1}. The atmospheric pressure fields used to compute gas saturations should also be consistent with the other physical forcing. Thus for the OMIP forced simulations, modelers will use surface atmospheric pressure from CORE II, converted to atm.

For the two abiotic carbon tracers, abbreviating $K' = K_0 C_f$, we can write their surface saturation concentrations (Eq. 14) as

$$20 \quad [CO_2^*]_{sat}^{abio} = K' \, (P_a - pH_2O) \, x_{CO_2} \quad (17)$$

and

$$\left[^{14}CO_2^*\right]_{sat}^{abio} = [CO_2^*]_{sat} \, ^{14}r'_{atm}. \quad (18)$$

Here $^{14}r'_{atm}$ represents the normalized atmospheric ratio of $^{14}C/C$, i.e.

$$^{14}r'_{atm} = \frac{^{14}r_{atm}}{^{14}r_{std}} = \left(1 + \frac{\Delta^{14}C_{atm}}{1000}\right), \quad (19)$$

25   where $^{14}r_{atm}$ is the atmospheric ratio of $^{14}C/C$, $^{14}r_{std}$ is the analogous ratio for the standard (1.170×10^{-12}, see Appendix A), and $\Delta^{14}C_{atm}$ is the atmospheric $\Delta^{14}C$, the fractionation-corrected ratio of $^{14}C/C$ relative to a standard reference given in permil (see below). We define $^{14}r'_{atm}$ and use it in Eq. (18) to be able to compare C_T^{abio} and $^{14}C_T^{abio}$, directly, potentially simplifying code verification and testing. With the above model formulation for the OMIP equilibrium run (where $xCO_2^{atm} = 284.65$ ppm and $\Delta^{14}C^{atm} = 0$ ‰), both C_T^{abio} and $^{14}C_T^{abio}$ have identical units. Short tests with the same initialization for

both tracers can thus verify consistency. Differences in the spin-up simulation will stem only from different initializations and radioactive decay. Differences will grow further during the anthropogenic perturbation (in *omip1-spunup*, i.e. after spin up), because of the sharp contrast between the shape of the atmospheric histories of $x\mathrm{CO}_2$ and $\Delta^{14}C_{atm}$.

For $^{13}\mathrm{C}$, the $\delta^{13}\mathrm{C}_{\mathrm{atm}}$ in atmospheric CO_2 is incorporated into Eq. (9) through the term $^{13}R_{\mathrm{atm}}$, which is given by

$$^{13}R_{\mathrm{atm}} = \left(\frac{\delta^{13}\mathrm{C}_{\mathrm{atm}}}{1000} + 1 \right) {}^{13}R_{std}, \tag{20}$$

where $^{13}R_{\mathrm{std}}$ is the standard ratio 0.0112372 (Craig, 1957). In this formulation, unlike for $^{14}C_{\mathrm{T}}^{\mathrm{abio}}$, $^{13}C_{\mathrm{T}}$ is not normalized by the standard ratio. However, modeling groups may wish to simulate normalized $^{13}C_{\mathrm{T}}$, e.g. by including a factor of $1/^{13}R_{\mathrm{std}}$ analogous to the approach used for $^{13}C_{\mathrm{T}}^{\mathrm{abio}}$. Modeling groups that simulate $^{13}\mathrm{C}$ in OMIP must report non-normalized values of the concentration $^{13}C_{\mathrm{T}}$ and the air-sea flux $F_{^{13}\mathrm{CO}_2}$. No other $^{13}\mathrm{C}$ results are requested.

For all gases simulated in OMIP, the atmospheric saturation concentration $[A]_{sat}$ is computed using Eq. (16). For all gases except oxygen, the combined solubility function ϕ_A^0 is available, being computed each time step using modeled T and S with Eq. (15), the corresponding gas-specific coefficients (Table 2), and the atmospheric mole fraction of each gas x_A. The exception is O_2 because rather than x_A and ϕ_A^0, it is the reference saturation concentration $[\mathrm{O}_2]_{sat}^0$ that is available (Garcia and Gordon, 1992, equation 8, Table 1).

In all cases, the same P_a/P_a^0 term is used to account for effects of atmospheric pressure (Eq. 16). For P_a, modelers must use the fields of surface atmospheric pressure *(sap)* from CORE II, i.e. for OMIP's forced ocean simulations (*omip1* and *omip1-spunup*), whereas for any CMIP6 coupled simulation, modelers should use *sap* from the coupled atmospheric model.

To compute $[A]_{sat}$ then, we only need one additional type of information, namely the x_A's for each of CO_2, CFC-11, CFC-12, and SF_6 as well as corresponding atmospheric histories for carbon isotopes:

1. $x_{\mathrm{CFC\text{-}11}}$, $x_{\mathrm{CFC\text{-}12}}$, and x_{SF_6}: Atmospheric records for observed CFC-11 and CFC-12 (in parts per trillion - ppt) are based on station data at 41°S and 45°N from (Walker et al., 2000) with subsequent extensions as compiled by Bullister (2015). For OMIP, each station will be treated as representative of its own hemisphere, except between 10°S and 10°N where those station values will be interpolated linearly as a function of latitude. Thus there are 3 zones: 90°S–10°S, where CFC's are held to same value as at the station at 41°S; 10°S–10°N, a buffer zone where values are interpolated linearly; and 10°N–90°N, where values are held to the same value as at the measuring station at 45°N. For SF_6, OMIP also relies on the Bullister (2015) synthesis over the same latitudinal bands. Values for all three inert chemical tracers are given at mid-year. It is recommended that modelers linearly interpolate these mid-year values to each time step, because annual growth rates can be large and variable.

2. x_{CO_2}: In the *spin-up* simulation, needed to initialize *omip1-spunup* simulation, atmospheric CO_2 is held constant at $x_{\mathrm{CO}_2} = 284.65$ ppm, the same preindustrial value as used for the CMIP6 *picontrol* simulation. Over the industrial era, defined as between years 1850.0 and 2010.0 for both of OMIP's transient simulations (*omip1* and *omip1-spunup*), atmospheric x_{CO_2} will follow the same observed historical increase as provided for CMIP6 (Meinshausen et al., 2016). Modelers should use the record of global annual mean atmospheric x_{CO_2}, interpolated to each time step. That increas-

ing x_{CO_2} affects the total tracer C_T in both transient simulations as well as the two abiotic tracers and $^{13}C_T$ in the *omip1-spunup* simulation. However, it does not affect the natural tracer C_T^{nat}, for which the atmosphere is always held at $x_{CO_2} = 284.65$ ppm.

3. $\Delta^{14}C^{atm}$: For the OMIP spin-up simulation, $\Delta^{14}C^{atm}$ is held constant at 0‰. For the *omip1-spunup* simulation, the

5   equilibrium reference is thus year 1850.0. Then the model must be integrated until 2010.0 following the observed record of $\Delta^{14}C^{atm}$ (Levin et al., 2010), separated into three latitudinal bands (90°S–20°S, 20°S–20°N, and 20°N–90°N).

4. $\delta^{13}C^{atm}$: The atmospheric record of $\delta^{13}C$ is the same as adopted for C4MIP, a compilation of ice-core data (Rubino et al., 2013) and atmospheric measurements at Mauna Loa (Keeling, 2001).

2.5.4   Surface ocean concentration

10   The equation above for the atmospheric equilibrium (saturation) concentration of a gas (Eq. 14) should not be confused with the analogous equation for the simulated ocean concentration. The surface-ocean equation allows conversion between the simulated surface-ocean dissolved gas concentration $[A]$, the corresponding fugacity f_O, and the partial pressure p_O of the surface ocean as follows:

$$[A] = K_0\, f_O = K_0\, C_f\, p_O = K'\, p_O. \qquad (21)$$

15   This surface-ocean equation is analogous to that for the atmospheric equilibrium saturation concentration $[A]_{sat}$ (Eq. 14), except that the ocean equation omits the final portion of the atmospheric equation which computes the mole fraction, a conventional parameter only for the atmosphere. Thus the combined term that includes the atmospheric pressure and humidity corrections (last term in parentheses) in Eq. (14) is not pertinent for the surface ocean equation. It should not be used when converting between simulated oceanic $[A]$ and the corresponding p_O. Confusion on this point was apparent in the publicly

20   available OMIP2 code, i.e. for the conversion from $[CO_2^*]$ to pCO_2, although that did not affect simulated F_{CO_2}.

     To avoid potential confusion and redundancy, OMIP modelers may prefer to separately compute the parts of ϕ_A rather than computing ϕ_A^0 and using it directly. Since

$$\phi_A = K_0\, C_f\, (P_a - pH_2O) = K'\, (P_a - pH_2O), \qquad (22)$$

modelers need only compute K', and use that in both the ocean equation (Eq. 21) and the atmospheric saturation equation

25   (Eq. 14), while for the latter also correct for atmospheric pressure and humidity, i.e. the $(P_a - pH_2O)$ term. That combined correction is to be computed with P_a from the CORE II forcing and with pH_2O calculated from model surface T and S (Weiss and Price, 1980, Eq. 10):

$$pH_2O = 24.4543 - 67.4509 \left(\frac{100}{T}\right) - 4.8489\, ln\left(\frac{T}{100}\right) - 0.000544\, S, \qquad (23)$$

where pH_2O is in atm, T is the in-situ, absolute temperature and S is salinity in permil. In this way, OMIP modelers may avoid

30   using the sometimes confusing combined term ϕ_A^0 altogether as well as its approximative pressure correction when calculating

the saturation concentration (Eq. 16). Pressure corrections for K' may be neglected in the surface ocean where total pressure remains close to 1 atm (Weiss, 1974).

The ocean equation (Eq. 21) converts a simulated dissolved gas concentration to a partial pressure using its combined product K', which can be computed directly for some gases or via a two-step process for others. For OMIP's inert chemical tracers,

5   tabulated coefficients can be used to compute K' directly, i.e. for CFC-11 and CFC-12 (Warner and Weiss, 1985, Table 2) and for SF_6 (Bullister et al., 2002, Table 2) using modeled T and S in an equation just like Eq. 15 but without the first T^2 term ($a_4 = 0$):

$$ln(K') = a_1 + a_2 \left(\frac{100}{T} \right) + a_3\, ln \left(\frac{T}{100} \right) + S \left[b_1 + b_2 \left(\frac{T}{100} \right) + b_3 \left(\frac{T}{100} \right)^2 \right], \tag{24}$$

where T is the in-situ absolute temperature and S is salinity in permil.

10   For O_2, K' is not needed for the saturation calculations, but it is necessary when using the simulated dissolved $[O_2]$ to compute the corresponding surface ocean pO_2, a required variable for OMIP and CMIP6. That solubility conversion factor K' can be derived by substituting its definition into Eq. (14) and rearranging, so that

$$K'_{O2} = \frac{[O_2]^0_{sat}}{x_{O_2}(P_a^0 - pH_2O)}, \tag{25}$$

where the numerator is from Eq. 8 of Garcia and Gordon (1992) using coefficients from their Table 1, and the denominator is

15   the product of the corresponding constant atmospheric mole fraction of O_2 ($x_{O_2} = O.20946$) and the wet-to-dry correction at 1 atm as described above. The computed K'_{O2} is then exploited to compute the partial pressure of oxygen ($pO_2 = [O_2]/K'_{O2}$).

For CO_2, tabulated coefficients are not available to compute K', but they are available to compute K_0 (Weiss, 1974, Table 1). Hence given that $K' = K_0\, C_f$, modelers must also compute the fugacity coefficient C_f from Eq. 9 of Weiss (1974):

$$C_f = exp \left[\left(B + 2\, x_2^2\, \delta_{12} \right) \frac{P_{ao}}{RT} \right], \tag{26}$$

20   where B is the virial coefficient of CO_2 (Weiss, 1974, Eq. 6), x_2 is the sum of the mole fractions of all remaining gases ($1 - xCO_2$, when $xCO_2 \ll 1$), and $\delta_{12} = 57.7 - 0.118T$. Here P_{ao} is the total pressure (atmospheric + hydrostatic) in atm, R is the gas constant ($82.05736\,cm^3\,atm\,mol^{-1}\,K^{-1}$), and T is the in-situ absolute temperature (K).

Although the surface ocean concentration of dissolved carbon dioxide gas $[CO_2^*]$ is needed to compute air-sea CO_2 exchange, it is not that inorganic carbon species that is carried as a tracer in ocean carbon models (Sect. 2.6). Instead the $[CO_2^*]$

25   concentration ($mol\,m^{-3}$) must be computed each time step from a model's simulated surface C_T, A_T, T, and S as well as nutrient concentrations (total dissolved inorganic phosphorus P_T and silicon Si_T) as detailed in the following section. All OMIP biogeochemical models will carry C_T and A_T as passive tracers. Most if not all will also carry at least one inorganic nutrient, nitrogen or phosphorus. Some will carry silicon. For models that carry only nitrogen, it is preferred that they compute P_T by dividing the total dissolved inorganic nitrogen concentration by 16, the constant N:P ratio from Redfield et al. (1963). For

30   models without Si_T, it is preferred that they use climatological Si_T data interpolated to their model grid (i.e. annual average data from WOA2013). These options offer a better alternative than assuming nutrient concentrations are zero, which lead to systematic shifts of order of $10\,\mu$atm in calculated surface-water pCO_2.

The abiotic portion of the biogeochemical simulation, carries only two tracers, C_T^{abio} and $^{14}C_T^{abio}$, which are not connected to other biogeochemical tracers. Hence to compute corresponding abiotic $[CO_2^*]$ and $[^{14}CO_2^*]$ concentrations, we also need abiotic alkalinity. Following OCMIP2, the abiotic alkalinity in OMIP will be calculated simply as a normalized linear function of salinity:

$$A_T^{abio} = \overline{A_T} * \frac{S}{\overline{S}},\qquad(27)$$

where $\overline{A_T}$ is the global mean of surface observations 2297 μmol kg^{-1} (Lauvset et al., 2016) and $\overline{S}$ is the model's global- and annual-mean surface salinity. In practice, it is recommended that $\overline{S}$ is first computed as the global mean of the initial salinity field and then, after one year of simulation, from the annual mean salinity of the previous year. Also needed are two other input arguments, P_T and Si_T. Although accounting for both of their acid systems makes a difference, these abiotic tracers are not included along with abiotic C_T. Hence we take their concentrations as being constant, equal to the global mean of surface observations for P_T of 0.5 μmol kg^{-1} and for Si_T of 7.5 μmol kg^{-1}. The assumption of constant nutrient distributions applies only to the carbonate chemistry calculations for abiotic C_T.

For the abiotic simulation's radiocarbon tracer, we must likewise compute its surface-ocean dissolved gas concentration $[^{14}CO_2^*]$. The latter is related to the calculated dissolved gas concentration of the stable abiotic carbon tracer as follows:

$$\left[^{14}CO_2^*\right]^{abio} = [CO_2^*]^{abio}\ ^{14}r'_{ocn},\qquad(28)$$

where

$$^{14}r'_{ocn} = \frac{^{14}r_{ocn}}{^{14}r_{std}} = \frac{^{14}C_T^{abio}}{C_T^{abio}}\qquad(29)$$

and $^{14}r_{ocn}$ is the ^{14}C/C of seawater. This normalization essentially means that $^{14}C_T^{abio}$ represents the actual fractionation-corrected ^{14}C concentration divided by $^{14}r_{std}$. This output must be saved in normalized form. But for subsequent ^{14}C budget calculations, it will be necessary to back-correct the normalized and fractionation-corrected modeled concentration ($^{14}C_T^{abio}$) and ^{14}C flux ($F_{^{14}CO_2}^{abio}$), i.e. the only two ^{14}C variables saved in OMIP, to molar units of actual ^{14}C (see Appendix A). For eventual comparison to ocean measurements, one can compute oceanic $\Delta^{14}C$ as

$$\Delta^{14}C_{ocn}^{abio} = 1000\left(^{14}r'_{ocn} - 1\right).\qquad(30)$$

For ^{13}C, the surface ocean dissolved gas concentration $[^{13}CO_2^*]$ is given by

$$\left[^{13}CO_2^*\right] = [CO_2^*]\ ^{13}r_{ocn},\qquad(31)$$

where $^{13}r_{ocn} =\ ^{13}C_T/C_T$. Here $^{13}C_T$ is not normalized by the standard ratio, but modeling groups may wish to simulate normalized $^{13}C_T$ by including a factor of $1/^{13}r_{std}$, analogous to what is done for the $^{14}C_T^{abio}$ normalization above.

2.6 Carbonate chemistry

Unlike other modelled gases in OMIP, CO_2 does not occur in seawater as a simple dissolved passive tracer. Instead, it reacts with seawater forming carbonic acid (H_2CO_3), most of which dissociates into two other inorganic species, bicarbonate

(HCO$_3^-$) and carbonate (CO$_3^{2-}$) ions. Since dissolved CO$_2$ cannot be distinguished analytically from the much less abundant H$_2$CO$_3$, common practice is to refer to the sum of the two, CO$_2$ + H$_2$CO$_3$, as CO$_2^*$. The sum of the three species CO$_2^*$ + HCO$_3^-$ + CO$_3^{2-}$ is referred to as total dissolved inorganic carbon C_T, while their partitioning depends on seawater pH, temperature, salinity, and pressure. The pH may be calculated from C_T and seawater's ionic charge balance, formalised as

5 total alkalinity A_T. Both C_T and A_T are conservative with respect to mixing and changes in seawater temperature, salinity, and pressure. Hence both are carried as passive tracers in all ocean models, and both are used, along with temperature, salinity, and nutrient concentrations, to compute the dissolved concentration of CO$_2$ and the related pCO$_2$, as needed to compute air-sea CO$_2$ fluxes.

To simulate carbonate chemistry, OMIP groups should use the total pH scale and the equilibrium constants recommended for

10 best practices (Dickson et al., 2007; Dickson, 2010). Additionally, the model's total alkalinity equation should include alkalinity from phosphoric and silicic acid systems as well as from carbonic acid, boric acid, and water. Neglect of the former two acid systems, which we refer to as phosphorus and silicon alkalinity, is common among model groups but leads to systematic errors in computed pCO$_2$, e.g. in the Southern Ocean (Najjar and Orr, 1998; Orr et al., 2015). Models with the nitrogen cycle should also account for effects of changes in nitrogen speciation on total alkalinity, including changes due to denitrification

15 and nitrogen fixation plus nitrification. Models that have P_T but not nitrogen as a nutrient should model impacts of nitrate on alkalinity by multiplying $J_{PO_4^{3-}}$ by 16.

Although phosphorus and silicon alkalinity is included in the carbonate chemistry routines provided for OCMIP2 and OCMIP3 (Orr et al., 1999b; Aumont et al., 2004), those routines focused only on computing surface pCO$_2$ and are now outdated. They have been replaced by *mocsy*, a new Fortran 95 package for ocean modelers (Orr and Epitalon, 2015). Relative

20 to the former OCMIP code, *mocsy* computes derived variables (e.g. pCO$_2$, pH, CO$_3^{2-}$, and CaCO$_3$ saturation states) throughout the water column, corrects for common errors in pressure corrections, and replaces the solver of the pH-Alkalinity equation with the faster and safer SolveSaphe algorithm from Munhoven (2013). The latter converges under all conditions, even for very low salinity (low C_T and A_T), unlike other approaches. The *mocsy* routines may be downloaded by issuing the following command:

25 `git clone https://github.com/jamesorr/mocsy.git`

and then installed by typing make. Alternatively, it can be dowloaded directly from the same site as a zipfile.

3 Diagnostics

The second goal of OMIP-BGC is to provide a complete list of diagnostics requested for the ocean simulations of inert chemistry and biogeochemistry within the framework of OMIP and CMIP6. The limited diagnostics requested for the simulations

30 of inert chemistry are provided in Table 4. The diagnostics requested for the biogeochemical simulations are more extensive. Hence they are given here as a series of tables separated by priority, type, and output frequency, i.e. as annual means (Tables 5 to 8) and monthly means (Tables 9 to 14). The same list of requested variables is given in a different form and with more

detail in the OMIP-BGC MIP tables for CMIP6, which will be made available online (as an Excel spreadsheet) from either the CMIP6 web site or the OMIP-BGC web site (see Sect. 5).

4   Conclusions

The required OMIP simulation *(omip1)* will be performed by many groups, each of which will couple their global-ocean, sea-ice model to a passive-tracer transport model for inert chemistry and ocean biogeochemistry, online. All groups, even those without biogeochemistry, will include at least one inert chemistry tracer (CFC-12) to assess subsurface model ventilation; two other tracers (CFC-11 and SF_6) are also requested to better assess subsurface watermass ages relative to observations. Groups with ocean biogeochemical models should also include that component (OMIP-BGC). The physical component will be forced with the CORE II forcing (1948–2009) over five repeated cycles (310 years) as described in the companion OMIP paper (Griffies et al., 2016). The biogeochemical component will be connected for the full 310 yr. Each model's atmospheric CO_2 will be held to the CMIP6 preindustrial level (1 January 1850) during the first 150 years (1700–1849), while for the next 160 years (1850-2009) models will be forced to follow the historical observations as defined for CMIP6. Physical analyses will focus on the fifth cycle, while those for the chemistry and biogeochemistry will also study transient changes over the industrial era. It is critical that all OMIP-BGC simulations include the *natural* carbon tracer C_T^{nat} to assess and remove effects of model drift.

An optional simulation *(omip1-spunup)* is requested from all groups having biogeochemistry able to afford a long spin up, made beforehand. Rather than using observed climatologies to initialize the biogeochemistry as in *omip1*, this simulation will be initialized with model tracer fields that have been spun up preferably for 2000 years or more. In addition, the *omip1-spunup* simulation (and its spin up) will include two simplified tracers, abiotic carbon and radiocarbon, to evaluate deep-ocean circulation and deconvolve physical vs. biological contributions to the carbon cycle. Finally, groups already having ^{13}C as a biogeochemical tracer are encouraged to include that in the *omip1-spunup* simulation, using commmon OMIP formulations for gas exchange and fractionation, to evaluate the simulated Suess effect and to compare cycling of ^{13}C in the marine ecosystem. Besides the initial fields and the three new tracers, the *omip1* and *omip1-spunup* simulation protocols are identical.

5   Data and code availability

To facilitate comparison, an OMIP-BGC web page (http://omip-bgc.lsce.ipsl.fr), now under construction, will provide links to these protocols as well as links to distribute OMIP-BGC's common atmospheric gas histories, data fields for initialization, and code to compute all facets of gas exchange and carbonate chemistry. This site will be open for public use within 4 weeks after publication of this Discussion manuscript, all data files and code will be made available there by the time that the revised version manuscript is submitted. The code currently mentioned in this manuscript is available in the *mocsy* package, which can be obtained as detailed in Sect. 2.6. That package contains not only the carbonate chemistry routines, but also routines in the

gasx module to compute Schmidt numbers, solubilities, and air-sea exchange for the gases to be modeled during OMIP (CO_2, O_2, CFC-11, CFC-12, and SF_6).

Appendix A: Converting modeled ^{14}C fluxes to conventional units

The ^{14}C tracer that is adopted for OMIP from OCMIP is fractionation corrected to avoid the need to explicitly compute ^{13}C fluxes between modeled carbon reservoirs. It is also normalized. Both of these manipulations affect the units of modeled ^{14}C concentrations and fluxes. These normalized, fractionation-corrected units must be used when OMIP model groups save their ^{14}C output. The saved OMIP model output is used directly to calculate simulated $\Delta^{14}C_{\text{ocn}}$ with Eqs. (29) and (30) for comparison to observations, but for budget calculations it must be converted to atoms or moles of ^{14}C (Naegler, 2009). Here we detail that conversion.

As mentioned in Sects. 2.5.3 and 2.5.4, modeled ^{14}C ratios in OMIP are expressed relative to total carbon, i.e. the *fractional isotopic abundance* $^{14}r_{\text{model}} = {}^{14}\text{C}/\text{C}$; conversely, for ^{13}C, its ratio is typically shown relative to ^{12}C (Mook, 1986), i.e. with the *isotopic ratio* $^{13}R = {}^{13}\text{C}/{}^{12}\text{C}$. The *fractional abundance* approach is convenient for ocean carbon-cycle models, which already transport total carbon, e.g. to assess uptake of fossil CO_2, which includes both ^{12}C and ^{13}C. But whether ^{12}C or C is the reference, there is only a small effect on simulated results. That is, ^{13}C amounts to only about 1% of the total carbon ($^{13}R_{\text{std}} = 0.0112372$, Craig, 1957) and ^{14}C is proportionally much less still. For ^{14}C, we adopt as a reference the standard isotopic fractional abundance $^{14}r_{\text{std}}$ ($^{14}\text{C}/\text{C}$) of 1.170×10^{-12}, which follows from the absolute international standard activity for $^{14}r_{\text{std}}$ of 13.56 ± 0.07 disintegrations per minute (dpm) per g C (Karlen et al., 1965) and a radiocarbon half-life of 5700 ± 30 yr (Audi et al., 2003; Bé et al., 2013). For comparison, Karlen et al. (1965) used the now outdated value for the half-life (5730 ± 40 yr, Godwin, 1962) to infer that $^{14}r_{\text{std}} = 1.176 \times 10^{-12}$; both of those values should now be revised downward to the values provided in the previous sentence.

The purpose of Δ^{14}C and the fractionation-normalized ratio $^{14}r_N$ is to remove the impact of isotopic fractionation to isolate the effect of "aging" by radioactive decay. Such fractionation occurs during photosynthesis and air-sea CO_2 exchange, leading to differences in the $^{13}\text{C}/{}^{12}\text{C}$ signature in different reservoirs; without fractionation, that ratio would not differ between carbon reservoirs. Fractionation of ^{14}C is about twice that of ^{13}C in permil units, based on the atomic mass difference relative to ^{12}C. One can approximately remove the influence of fractionation on ^{14}C by relying on measured δ^{13}C referenced to a common isotopic δ^{13}C signature, taken as -25‰ (Broecker and Olson, 1961). Thus for a particular reservoir i where $^{14}r_i = {}^{14}\text{C}/\text{C}$:

$$^{14}r_{\text{N,i}} = {}^{14}r_{\text{i}} \left[1 - 2 \left(\frac{\delta^{13}\text{C}_{\text{i}} + 25}{1000} \right) \right], \tag{A1}$$

where the two terms in the numerator in parentheses are in permil, and

$$\Delta^{14}\text{C}_i = \left(\frac{^{14}r_{\text{N,i}}}{^{14}r_{\text{std}}} - 1 \right) 1000. \tag{A2}$$

Deviations between this correction and the actual impact of fractionation on ^{14}C occur under non-steady state conditions. More importantly, radioactive decay in the ocean results in a net transfer of ^{14}C into the ocean, unlike the case for ^{13}C, and this

net ^{14}C flux is not corrected for fractionation. In OMIP, we simplify equations and avoid small numerical values by defining $^{14}r' = {}^{14}r/^{14}r_{\text{std}}$, i.e. compare Eq. (A2) with Eq. (30). This normalization is further discussed in Sects. 2.5.3 and 2.5.4 (see in particular in Eqs. (19) and (29)).

Thus OMIP simulates a ^{14}C concentration that is (1) fractionation corrected and (2) normalized by dividing ^{14}r by $^{14}r_{\text{std}}$. These corrections must be removed to convert modeled concentrations into number of atoms or moles of ^{14}C. Thus, we rearrange Eq. (A1) while multiplying by the common denominator (C) of both its ^{14}r values and then we multiply by $^{14}r_{\text{std}}$, yielding

$$^{14}\text{C} = \left({}^{14}\text{C}_{\text{model}} \Big/ \left[1 - 2 \left(\frac{(\delta^{13}\text{C} + 25)}{1000} \right) \right] \right) {}^{14}r_{\text{std}}. \tag{A3}$$

Here we neglect that the δ^{13}C of the standard material ($-19‰$, Karlen et al., 1965) differs from that of ocean water (-1 to $2‰$) because the resulting bias in computed ^{14}C is only 0.02 %.

Now let us use Eq. (A3) to compute corrections for the preindustrial ocean and atmosphere by plugging in their estimated δ^{13}C values. For the preindustrial ocean, we assume that δ^{13}C was around $2‰$ in surface waters and $0‰$ in the deep ocean, a difference attributable to biological fractionation. Inserting those numbers into Eq. (A3) and simplifying, we thus have

$$^{14}\text{C}_S \approx {}^{14}\text{C}_{\text{model},S} \left(1 + \frac{54}{1000} \right) {}^{14}r_{\text{std}} \tag{A4a}$$

$$^{14}\text{C}_D \approx {}^{14}\text{C}_{\text{model},D} \left(1 + \frac{50}{1000} \right) {}^{14}r_{\text{std}}, \tag{A4b}$$

where the subscripts S and D indicate surface and deep waters. Thus, there is a correction of $54‰$ for the surface ocean and $50‰$ for the deep ocean. For the preindustrial atmosphere, using the same approach with its assumed δ^{13}C of -6.4‰, we find

$$^{14}\text{C}_A \approx {}^{14}\text{C}_{\text{model},A} \left(1 + \frac{37}{1000} \right) {}^{14}r_{\text{std}}. \tag{A5}$$

Thus, the ^{14}C$_A$ correction to switch from model to conventional units for the atmosphere is about $37‰$.

Turning to the gas exchange, in the model formulation the related change in the atmospheric ^{14}C inventory is calculated by removing the net air-to-sea flux $F^{\text{abio}}_{^{14}\text{CO}_2}$ and adding that to the ocean ^{14}C inventory. To convert this modeled air-sea flux into atomic units, we use the same correction as for the modeled concentrations because the change in inventory is proportional to the change in concentrations. The difference between the atmospheric and oceanic corrections ($54 - 37 = 17‰$) is related to the equilibrium fractionation factor for air-sea transfer, i.e. 8–9‰ for ^{13}C and double that for ^{14}C. In the model, the impact of fractionation on the net (non-zero) radiocarbon transfer is not taken explicitly into account giving rise to this inconsistency even under equilibrium conditions where a climatological average flux replaces the ocean sink by radioactive decay.

In the OMIP simulations, atmospheric radiocarbon is prescribed and forces the ocean. The ocean radiocarbon inventory changes in response to this forcing. Thus, a correction of about $+50‰$ (Eqs. (A4a) and (A4b)) is needed to convert ocean ^{14}C concentrations and net air-sea ^{14}C fluxes from model units into molar units. For concentrations,

$$^{14}\text{C}_{\text{T}} = {}^{14}\text{C}^{\text{abio}}_{\text{T, model}} \times 1.05 \times 1.170 \times 10^{-12}, \tag{A6}$$

and for fluxes,

$$F_{^{14}CO_2} = F_{^{14}CO_2,\text{model}}^{\text{abio}} \times 1.05 \times 1.170 \times 10^{-12}. \tag{A7}$$

In both Eqs. (A6) and (A7), units on the left-hand side are in terms of mol ^{14}C while those for the first term on the right-hand side are model units (*normalized* and *fractionation-corrected* mol ^{14}C).

5   *Acknowledgements.* JCO and LB were supported by the EU H2020 CRESCENDO project (grant 641816). JLB was supported by NOAA's Climate Program Office—this is PMEL contribution #4476. HG was supported by a Marie Curie Career Integration Grant from the European Commission. RGN was supported by NASA's Ocean Biology and Biogeochemistry Program and NASA's Interdisciplinary Science Program.

References

Audi, G., Bersillon, O., Blachot, J., and Wapstra, A. H.: The NUBASE evaluation of nuclear and decay properties, Nuclear Physics A, 729, 3–128, 2003.

Aumont, O. and Bopp, L.: Globalizing results from ocean in situ iron fertilization studies,, Global Biogeochem. Cycles,, 20, GB2017, doi:10.1029/2005GB002591, 2006.

Aumont, O., Orr, J. C., Jamous, D., Monfray, P., Marti, O., and Madec, G.: A degradation approach to accelerate simulations to steady state in a 3-D tracer transport model of the global ocean, Clim. Dyn., 14, 101–116, 1998.

Aumont, O., Quéré, C. L., and Orr, J. C.: NOCES Interannual HOWTO. Internal NOCES/OCMIP report, LSCE/CEA Saclay, Gif-sur-Yvette, France, 2nd edn., http://ocmip5.ipsl.jussieu.fr/OCMIP/phase3/simulations/NOCES/HOWTO-NOCES.html, 2004.

Bacastow, R. and Maier-Reimer, E.: Ocean-circulation model of the carbon cycle, Clim. Dyn., 4, 95–125, 1990.

Bé, M., Chisté, V., Dulieu, C., Mougeot, X., Chechev, V., Kondev, F., Nichols, A., Huang, X., and Wang, B.: Table of Radionuclides (Comments on evaluations), Monographie BIPM-5, vol. 7, Bureau International des Poids et Mesure, Pavillon de Breteuil, Sèvres, France, 2013.

Bopp, L., Resplandy, L., Orr, J. C., Doney, S. C., Dunne, J. P., Gehlen, M., Halloran, P., Heinze, C., Ilyina, T., Séférian, R., Tjiputra, J., and Vichi, M.: Multiple stressors of ocean ecosystems in the 21st century: projections with CMIP5 models, Biogeosciences, 10, 6225–6245, doi:10.5194/bg–10–6225–2013, http://www.biogeosciences.net/10/6225/2013/, 2013.

Broecker, W. and Peng, T.: Tracers in the sea, Eldigio, Lamont-Doherty, Palisades, NY, 691pp, 1982.

Broecker, W. S. and Olson, E. A.: Lamont radiocarbon measurements VIII, Radiocarbon, 3, 176–204, 1961.

Broecker, W. S. and Peng, T.-H.: Gas exchange rates between air and sea, Tellus, 26, 21–35, 1974.

Bullister, J.: Atmospheric Histories (1765-2015) for CFC-11, CFC-12, CFC-113, CCl4, SF6 and N2O, Carbon Dioxide Information Analysis Center, Oak Ridge National Laboratory, U.S. Department of Energy, Oak Ridge, Tennessee, http://cdiac.ornl.gov/ftp/oceans/CFC_ATM_Hist/CFC_ATM_Hist_2015, 2015.

Bullister, J. L., Wisegarver, D. P., and Menzia, F. A.: The solubility of sulfur hexafluoride in water and seawater, Deep-Sea Res. I, 49, 175–187, 2002.

Craig, H.: Isotopic standards for carbon and oxygen and correction factors for mass-spectrometric analysis of carbon dioxide, Geochim. Cosmochim. Acta, 12, 133–149, 1957.

Dickson, A. G.: The carbon dioxide system in seawater: equilibrium chemistry and measurements, in: Guide to best practices for ocean acidification research and data reporting, edited by Riebesell, U., Fabry, V. J., Hansson, L., and Gattuso, J.-P., pp. 17–40, Publications Office of the European Union, 2010.

Dickson, A. G., Sabine, C. L., and Christian, J. R.: Guide to best practices for ocean CO_2 measurements, , PICES Special Publication 3, 191 pp., http://aquaticcommons.org/1443/, 2007.

Dlugokencky, E. and Tans, P.: Trends in atmospheric carbon dioxide, National Oceanic & Atmospheric Administration, Earth System Research Laboratory (NOAA/ESRL), available at: http://www.esrl.noaa.gov/gmd/ccgg/trends, 2016.

Doney, S., Lindsay, K., Caldeira, K., Campin, J.-M., Drange, H., Dutay, J.-C., Follows, M., Gao, Y., Gnanadesikan, A., Gruber, N., Ishida, A., Joos, F., Madec, G., Maier-Reimer, E., Marshall, J., Matear, R., Monfray, P., Mouchet, A., Najjar, R., Orr, J., Plattner, G.-K., Sarmiento, J., Schlitzer, R., Slater, R., Totterdell, I., Weirig, M.-F., Yamanaka, Y., and Yool, A.: Evaluating Global Ocean Carbon Models: The Importance of Realistic Physics, Global Biogeochem. Cy., 18, GB3017, doi:10.1029/2003GB002150, 2004.

Dufour, C. O., Sommer, J. L., Gehlen, M., Orr, J. C., Molines, J.-M., Simeon, J., and Barnier, B.: Eddy compensation and controls of the enhanced sea-to-air CO_2 flux during positive phases of the Southern Annular Mode, Global Biogeochem. Cycles, 27, 950–961, doi:10.1002/gbc.20090, 2013.

Dutay, J.-C., Bullister, J., Doney, S. C., Orr, J. C., Najjar, R. G., Caldeira, K., Campin, J.-M., Drange, H., Follows, M., Gao, Y., Gruber, N., Hecht, M. W., Ishida, A., Joos, F., Lindsay, K., Madec, G., Maier-Reimer, E., Marshall, J. C., Matear, R., Monfray, P., Mouchet, A., Plattner, G. K., Sarmiento, J. L., Schlitzer, R., Slater, R. D., Totterdell, I. J., Weirig, M.-F., Yamanaka, Y., and Yool, A.: Evaluation of ocean model ventilation with CFC-11: Comparison of 13 global ocean models, Ocean Modelling, 4, 89–120, 2002.

Dutay, J.-C., Jean-Baptiste, P., Campin, J.-M., Ishida, A., Maier-Reimer, E., Matear, R., Mouchet, A., Totterdell, I., Yamanaka, Y., Rodgers, K., Madec, G., and Orr, J.: Evaluation of OCMIP-2 ocean models' deep circulation with mantle helium-3, J. Mar. Systems, 48, 15–36, doi:10.1016/j.jmarsys.2003.05.010, doi:10.1016/j.jmarsys.2003.05.010, 2004.

Eyring, V., Bony, S., Meehl, G. A., Senior, C. A., Stevens, B., Stouffer, R. J., and Taylor, K. E.: Overview of the Coupled Model Intercomparison Project Phase 6 (CMIP6) experimental design and organization, Geoscientific Model Development, 9, 1937–1958, doi:10.5194/gmd–9–1937–2016, 2016.

Garcia, H. E. and Gordon, L. I.: Oxygen solubility in seawater: Better fitting equations, Limnol. Oceanogr., 37, 1307–1312, 1992.

Garcia, H. E., Locarnini, R. A., Boyer, T. P., Antonov, J. I., Baranova, O., Zweng, M., Reagan, J., and Johnson, D.: World Ocean Atlas 2013, Volume 3: Dissolved Oxygen, Apparent Oxygen Utilization, and Oxygen Saturation, edited by S. Levitus and A. Mishonov, Atlas NESDIS 75, NOAA, U.S. Government Printing Office, Washington, D.C., 27 pp., 2014a.

Garcia, H. E., Locarnini, R. A., Boyer, T. P., Antonov, J. I., Baranova, O., Zweng, M., Reagan, J., and Johnson, D.: World Ocean Atlas 2013, Volume 4: Dissolved Inorganic Nutrients (phosphate, nitrate, silicate), edited by S. Levitus and A. Mishonov, Atlas NESDIS 76, NOAA, U.S. Government Printing Office, Washington, D.C., 25 pp., 2014b.

Godwin, H.: Half-life of radiocarbon, Nature, 195, 984, 1962.

Graven, H. D., Gruber, N., Key, R., Khatiwala, S., and Giraud, X.: Changing controls on oceanic radiocarbon: New insights on shallow-to-deep ocean exchange and anthropogenic CO_2 uptake, J. Geophys. Res., 117, C10005, doi:10.1029/2012JC008074, http://dx.doi.org/10.1029/2012JC008074, 2012.

Griffies, S. M., Danabasoglu, G., Durack, P. J., Adcroft, A. J., Balaji, V., Böning, C. W., Chassignet, E. P., Curchitser, E., Deshayes, J., Drange, H., Fox-Kemper, B., Gleckler, P. J., Gregory, J. M., Haak, H., Hallberg, R. W., Hewitt, H. T., Holland, D. M., Ilyina, T., Jungclaus, J. H., Komuro, Y., Krasting, J. P., Large, W. G., Marsland, S. J., Masina, S., McDougall, T. J., Nurser, A. J. G., Orr, J. C., Pirani, A., Qiao, F., Stouffer, R. J., Taylor, K. E., Treguier, A. M., Tsujino, H., Uotila, P., Valdivieso, M., Winton, M., and Yeager, S. G.: Experimental and diagnostic protocol for the physical component of the CMIP6 Ocean Model Intercomparison Project (OMIP), Geosci. Model Dev., in review, 1–108, doi:10.5194/gmd–2016–77, 2016.

Hansell, D. A., Carlson, C. A., Repeta, D. J., and Schlitzer, R.: Dissolved organic matter in the ocean: A controversy stimulates new insights, Oceanography, 22, 202–211, 2009.

Jahn, A., Lindsay, K., Giraud, X., Gruber, N., Otto-Bliesner, B. L., Liu, Z., and Brady, E. C.: Carbon isotopes in the ocean model of the Community Earth System Model (CESM1), Geoscientific Model Development, 8, 2419–2434, doi:10.5194/gmd–8–2419–2015, http://www.geosci-model-dev.net/8/2419/2015/, 2015.

Jones, C. D., Arora, V., Friedlingstein, P., Bopp, L., Brovkin, V., Dunne, J., Graven, H., Hoffman, F., Ilyina, T., John, J. G., Jung, M., Kawamiya, M., Koven, C., Pongratz, J., Raddatz, T., Randerson, J., and Zaehle, S.: The C4MIP experimental protocol for CMIP6, Geosci. Model Dev., submitted, 2016.

Joos, F., Orr, J. C., and Siegenthaler, U.: Ocean carbon transport in a box-diffusion versus a general circulation model, J. Geophys. Res., 102, 12 367–12 388, 1997.

Karlen, I., Olsson, I., Kallberg, P., and Kilicci, S.: Absolute determination of the activity of two C-14 dating standards, Arkiv Geofysik., 4, 465–471, 1965.

Keeling, C. D., Piper, S. C., Bacastow, R. B., Wahlen, M., Whorf, T. P., Heimann, M., and Meijer, H. A.: Exchanges of Atmospheric CO2 and 13CO2 with the Terrestrial Biosphere and Oceans from 1978 to 2000. I. Global Aspects, SIO Reference Series 01-06, Scripps Institution of Oceanography, San Diego, 2001.

Key, R. M., Sabine., C. L., Lee, K., Wanninkhof, R., Bullister, J., Feely, R. A., Millero, F. J., Mordy, C., and Peng, T.-H.: A Global Ocean Carbon Climatology: Results from Global Data Analysis Project (GLODAP), Global Biogeochem. Cy., 18, GB4031, doi:10.1029/2004GB002247, 2004.

Khatiwala, S.: Fast spin up of ocean biogeochemical models using matrix-free Newton–Krylov, Ocean Modelling, 23, 121–129, 2008.

Kwiatkowski, L., Yool, A., Allen, J. I., Anderson, T. R., Barciela, R., Buitenhuis, E. T., Butenschön, M., Enright, C., Halloran, P. R., Le Quéré, C., de Mora, L., Racault, M.-F., Sinha, B., Totterdell, I. J., and Cox, P. M.: iMarNet: an ocean biogeochemistry model intercomparison project within a common physical ocean modelling framework, Biogeosciences, 11, 7291–7304, doi:10.5194/bg–11–7291–2014, 2014.

Large, W. G. and Yeager, S. G.: The global climatology of an interannually varying air–sea flux data set, Climate Dynamics, 33, 341–364, 2009.

Lauvset, S. K., Key, R. M., Olsen, A., van Heuven, S., Velo, A., Lin, X., Schirnick, C., Kozyr, A., Tanhua, T., Hoppema, M., Jutterström, S., Steinfeldt, R., Jeansson, E., Ishii, M., Perez, F. F., Suzuki, T., and Watelet, S.: A new global interior ocean mapped climatology: the 1°x 1°GLODAP version 2, Earth Syst. Sci. Data Discuss., in review, 1–30, doi:10.5194/essd–2015–43, 2016.

Levin, I., Naegler, T., Kromer, B., Diehl, M., Francey, R. J., Gomez-Pelaez, A. J., Steele, L., Wagenbach, D., Weller, R., and Worthy, D. E.: Observations and modelling of the global distribution and long-term trend of atmospheric 14CO2, Tellus B, 62, 26–46, 2010.

Li, X. and Primeau, F. W.: A fast Newton–Krylov solver for seasonally varying global ocean biogeochemistry models, Ocean Modelling, 23, 13–20, 2008.

Matsumoto, K., Sarmiento, J. L., Key, R. M., Aumont, O., Bullister, J. L., Caldeira, K., Campin, J.-M., Doney, S. C., Drange, H., Dutay, J.-C., Follows, M., Gao, Y., Gnanadesikan, A., Gruber, N., Ishida, A., Joos, F., Lindsay, K., Maier-Reimer, E., Marshall, J. C., Matear, R. J., Monfray, P., Mouchet, A., Najjar, R., Plattner, G.-K., Schlitzer, R., Slater, R., Swathi, P. S., Totterdell, I. J., Weirig, M.-F., Yamanaka, Y., Yool, A., and Orr, J. C.: Evaluation of ocean carbon cycle models with data-based metrics, Geophys. Res. Lett., 31, L070303, doi:10.1029/2003GL018970, 2004.

Meinshausen, M., Vogel, E., Nauels, A., Lorbacher, K., Etheridge, D., Trudinger, C., Rayner, P., Fraser, P., Cannadell, P., Enting, I., and et al.: Historical greenhouse gas concentrations for CMIP6, Geosci. Model Dev. Disc., in prep., 2016.

Merlis, T. M. and Khatiwala, S.: Fast dynamical spin-up of ocean general circulation models using Newton–Krylov methods, Ocean Modelling, 21, 97–105, 2008.

Montzka, S., Fraser, P., Butler, J., Cunnold, D., Daniel, J., Derwent, R., Lal, S., McCulloch, A., Oram, D., Reeves, C., et al.: Scientific Assessment of Ozone Depletion, vol. 47, chap. Chapter 1: Controlled substances and other source gases, World Meteorol. Organ., Geneva, Switzerland, 2003.

Mook, W.: 13C in atmospheric CO2, Netherlands J. Sea Res., 20, 211–223, 1986.

Mouchet, A.: The ocean bomb radiocarbon inventory revisited, Radiocarbon, 55, 1580–1594, 2013.

Munhoven, G.: The mathematics of the total alkalinity—pH equation—pathway to robust and universal solution algorithms: the SolveSAPHE package v1.0.1, Geosci. Model Dev., 6, 1367–1388, doi:10.5194/gmd–6–1367–2013, 2013.

Naegler, T.: Reconciliation of excess 14C-constrained global CO2 piston velocity estimates, Tellus B, 61, 372–384, doi:10.1111/j.1600-0889.2008.00408.x, http://dx.doi.org/10.1111/j.1600-0889.2008.00408.x, 2009.

5 Najjar, R. and Orr, J.: Design of OCMIP-2 simulations of chlorofluorocarbons, the solubility pump and common biogeochemistry, Internal OCMIP Report, LSCE/CEA Saclay, Gif-sur-Yvette, France, http://ocmip5.ipsl.fr/documentation/OCMIP/phase2/simulations/design.ps, 1998.

Najjar, R. and Orr, J. C.: Biotic-HOWTO. Internal OCMIP Report, LSCE/CEA Saclay, Gif-sur-Yvette, France, 15 pp., http://ocmip5.ipsl.jussieu.fr/OCMIP/phase2/simulations/Biotic/HOWTO-Biotic.html, 1999.

10 Najjar, R. G., Jin, X., Louanchi, F., Aumont, O., Caldeira, K., Doney, S. C., Dutay, J.-C., Follows, M., Gruber, N., Joos, F., Lindsay, K., Maier-Reimer, E., Matear, R. J., Matsumoto, K., Monfray, P., Mouchet, A., Orr, J. C., Plattner, G.-K., Sarmiento, J. L., Schlitzer, R., Slater, R. D., ad Y. Yamanaka, M.-F. W., and Yool, A.: Impact of circulation on export production, dissolved organic matter, and dissolved oxygen in the ocean: Results from Phase II of the Ocean Carbon-cycle Model Intercomparison Project (OCMIP-2), Global Biogeochemical Cycles, 21, GB3007, doi:10.1029/2006GB002 857, 2007.

15 Oliver, K. I. C., Hoogakker, B. A. A., Crowhurst, S., Henderson, G. M., Rickaby, R. E. M., Edwards, N. R., and Elderfield, H.: A synthesis of marine sediment core δ^{13}C data over the last 150 000 years, Climate of the Past, 6, 645–673, doi:10.5194/cp–6–645–2010, http://www.clim-past.net/6/645/2010/, 2010.

Olsen, A., Key, R. M., van Heuven, S., Lauvset, S. K., Velo, A., Lin, X., Schirnick, C., Kozyr, A., Tanhua, T., Hoppema, M., Jutterström, S., Steinfeldt, R., Jeansson, E., Ishii, M., Pérez, F. F., and Suzuki, T.: An internally consistent data product for the world ocean: the Global
20 Ocean Data Analysis Project, version 2 (GLODAPv2), Earth Syst. Sci. Data Discuss., in review, 1–78, doi:10.5194/essd–2015–42, 2016.

Orr, J. C. and Epitalon, J.-M.: Improved routines to model the ocean carbonate system: mocsy 2.0, Geosci. Model Dev., 8, 485–499, doi:10.5194/gmd–8–485–2015, 2015.

Orr, J. C., Dutay, J.-C., Najjar, R., Bullister, J., and Brockmann, P.: CFC-HOWTO. Internal OCMIP Report, LSCE/CEA Saclay, Gif-sur-Yvette, France, 12 pp., http://ocmip5.ipsl.jussieu.fr/OCMIP/phase2/simulations/CFC/HOWTO-CFC.html, 1999a.

25 Orr, J. C., Najjar, R., Sabine, C. L., and Joos, F.: Abiotic-HOWTO. Internal OCMIP Report, LSCE/CEA Saclay, Gif-sur-Yvette, France, 25 pp., http://ocmip5.ipsl.jussieu.fr/OCMIP/phase2/simulations/Abiotic/HOWTO-Abiotic.html, 1999b.

Orr, J. C., Monfray, P., Maier-Reimer, E., Mikolajewicz, U., Palmer, J., Taylor, N. K., Toggweiler, J. R., Sarmiento, J. L., Quéré, C. L., Gruber, N., Sabine, C. L., Key, R. M., and Boutin, J.: Estimates of anthropogenic carbon uptake from four three-dimensionsal global ocean models, Global Biogeochem. Cy., 15, 43–60, 2001.

30 Orr, J. C., Fabry, V. J., Aumont, O., Bopp, L., Doney, S. C., Feely, R. A., Gnanadesikan, A., Gruber, N., Ishida, A., Joos, F., Key, R. M., Lindsay, K., Maier-Reimer, E., Matear, R., Monfray, P., Mouchet, A., Najjar, R. G., Plattner, G.-K., Rodgers, K. B., Sabine, C. L., Sarmiento, J. L., Schlitzer, R., Slater, R. D., Totterdell, I. J., Weirig, M.-F., Yamanaka, Y., and Yool, A.: Anthropogenic ocean acidification over the twenty-first century and its impact on calcifying organisms, Nature, 437, doi:10.1038/nature04 095, 681–686, 2005.

Orr, J. C., Gattuso, J.-P., and Epitalon, J.-M.: Comparison of ten packages that compute ocean carbonate chemistry, Biogeosciences, 12,
35 1483–1510, doi:10.5194/bg–12–1483–2015, 2015.

Peacock, S.: Debate over the ocean bomb radiocarbon sink: Closing the gap, Global Biogeochemical Cycles, 18, GB2022, doi:10.1029/2003GB002 211, 2004.

Quay, P., Sonnerup, R., Westby, T., Stutsman, J., and McNichol, A.: Changes in the 13C/12C of dissolved inorganic carbon in the ocean as a tracer of anthropogenic CO2 uptake, Global Biogeochemical Cycles, 17, 1004, doi:10.1029/2001GB001 817, 2003.

Quay, P. D., Tilbrook, B., and Wong, C.: Oceanic uptake of fossil fuel CO2: Carbon-13 evidence, Science, 256, 74–79, 1992.

Raynaud, S., Orr, J. C., Aumont, O., Rodgers, K. B., and Yiou, P.: Interannual-to-decadal variability of North Atlantic air-sea CO$_2$ fluxes, Ocean Sci., 2, 43–60, http://www.copernicus.org/EGU/os/os.html, 2006.

Redfield, A. C., Ketchum, B. H., and Richards, F.: The influence of organisms on the composition of sea water, in: The Sea, edited by Hill, M. N., vol. 2, pp. 26–77, Wiley-Interscience, New York, 1963.

Rigby, M., Prinn, R. G., O'Doherty, S., Montzka, S. A., McCulloch, A., Harth, C. M., Mühle, J., Salameh, P. K., Weiss, R. F., Young, D., Simmonds, P. G., Hall, B. D., Dutton, G. S., Nance, D., Mondeel, D. J., Elkins, J. W., Krummel, P. B., Steele, L. P., and Fraser, P. J.: Re-evaluation of the lifetimes of the major CFCs and CH3CCl3 using atmospheric trends, Atmospheric Chemistry and Physics, 13, 2691–2702, doi:10.5194/acp–13–2691–2013, 2013.

Rodgers, K. B., Aumont, O., Madec, G., Menkes, C., Blanke, B., Monfray, P., Orr, J. C., and Schrag, D. P.: Radiocarbon as a thermocline proxy for the eastern equatorial Pacific, Geophys. Res. Lett., 31, L14314, doi:10.1029/2004GL019764, 2004.

Roullet, G. and Madec, G.: Salt conservation, free surface, and varying levels: A new formulation for ocean general circulation models, J. Geophys. Res., 105, 23 927–23 942, doi:10.1029/2000JC900 089, 2000.

Rubino, M., Etheridge, D. M., Trudinger, C. M., Allison, C. E., Battle, M. O., Langenfelds, R. L., Steele, L. P., Curran, M., Bender, M., White, J. W. C., Jenk, T. M., Blunier, T., and Francey, R. J.: A revised 1000 year atmospheric δ13C-CO2 record from Law Dome and South Pole, Antarctica, J. Geophys. Res.: Atmospheres, 118, 8482–8499, doi:10.1002/jgrd.50 668, 2013.

Sarmiento, J. L., Monfray, P., Maier-Reimer, E., Aumont, O., Murnane, R., and Orr, J. C.: Sea-air CO$_2$ fluxes and carbon transport: A comparison of three ocean general circulation models, Global Biogeochem. Cy., 14, 1267–1281, 2000.

Schmitt, J., Schneider, R., Elsig, J., Leuenberger, D., Lourantou, A., Chappellaz, J., Köhler, P., Joos, F., Stocker, T. F., Leuenberger, M., et al.: Carbon isotope constraints on the deglacial CO2 rise from ice cores, Science, 336, 711–714, 2012.

Schmittner, A., Gruber, N., Mix, A. C., Key, R. M., Tagliabue, A., and Westberry, T. K.: Biology and air-sea gas exchange controls on the distribution of carbon isotope ratios (δ^{13}C) in the ocean, Biogeosciences, 10, 5793–2013, doi:10.5194/bg–10–5793–2013, 2013.

Séférian, R., Gehlen, M., Bopp, L., Resplandy, L., Orr, J. C., Marti, O., Dunne, J. P., Christian, J. R., Doney, S. C., Ilyina, T., Lindsay, K., Halloran, P., Heinze, C., Segschneider, J., and Tjiputra, J.: Inconsistent strategies to spin up models in CMIP5: implications for ocean biogeochemical model performance assessment, Geoscientific Model Development Discussions, 8, 8751–8808, doi:10.5194/gmdd–8–8751–2015, 2015.

Sweeney, C., Gloor, E., Jacobson, A. R., Key, R. M., McKinley, G., Sarmiento, J. L., and Wanninkhof, R.: Constraining global air-sea gas exchange for CO2 with recent bomb 14C measurements, Global Biogeochemical Cycles, 21, GB2015, doi:10.1029/2006GB002 784, 2007.

Tagliabue, A. and Bopp, L.: Towards understanding global variability in ocean carbon-13, Global Biogeochem. Cy., 22, GB1025, doi:10.1029/2007GB003 037, 2008.

Tagliabue, A., Aumont, O., DeAth, R., Dunne, J. P., Dutkiewicz, S., Galbraith, E., Misumi, K., Moore, J. K., Ridgwell, A., Sherman, E., et al.: How well do global ocean biogeochemistry models simulate dissolved iron distributions?, Global Biogeochem. Cy., 30, 149–174, 2015GB005 289, 10.1002/2015GB005 289, 2016.

Toggweiler, J. R., Dixon, K., and Bryan, K.: Simulations of radiocarbon in a coarse resolution world ocean model 1. Steady state prebomb distributions, J. Geophys. Res., 94, 8217–8242, 1989a.

Toggweiler, J. R., Dixon, K., and Bryan, K.: Simulations of radiocarbon in a coarse resolution world ocean model 2. Distributions of bomb-produced carbon 14, J. Geophys. Res., 94, 8243–8264, 1989b.

Walker, S. J., Weiss, R. F., and Salameh, P. K.: Reconstructed histories of the annual mean atmospheric mole fractions for the halocarbons CFC-11 CFC-12, CFC-113, and carbon tetrachloride, J. Geophys. Res., 105, 14 285–14 296, doi:10.1029/1999JC900 273, 2000.

5 Wanninkhof, R.: Relationship between wind speed and gas exchange over the ocean, J. Geophys. Res., 97, 7373–7382, 1992.

Wanninkhof, R.: Relationship between wind speed and gas exchange over the ocean revisited, Limnol. Oceanogr. Methods, 12, 351–362, 2014.

Warner, M. J. and Weiss, R. F.: Solubilities of chlorofluorocarbons 11 and 12 in water and seawater, Deep-Sea Res. Part A., 32, 1485–1497, 1985.

10 Waugh, D. W., Hall, T. M., and Haine, T. W. N.: Relationship among tracer ages, J. Geophys. Res., 108, doi:10.1029/2002JC001 325, 2003.

Weiss, R. F.: Carbon dioxide in water and seawater: the solubility of a non-ideal gas, Mar. Chem., 2, 203–215, 1974.

Weiss, R. F. and Price, B. A.: Nitrous oxide solubility in water and seawater, Mar. Chem., 8, 347–359, 1980.

Yool, A., Oschlies, A., Nurser, A. J. G., and Gruber, N.: A model-based assessment of the TrOCA approach for estimating anthropogenic carbon in the ocean, Biogeosciences, 7, 723–751, doi:10.5194/bg–7–723–2010, 2010.

15 Zhang, J., Quay, P. D., and Wilbur, D. O.: Carbon isotope fractionation during gas-water exchange and dissolution of CO 2, Geochimica et Cosmochimica Acta, 59, 107–114, 1995.

Table 1. Seawater coefficients for fit of Sc to temperature[*,†] from Wanninkhof (2014).

Gas	A	B	C	D	E	Sc (20°C)
CFC-11	3579.2	−222.63	7.5749	−0.14595	0.0011874	1179
CFC-12	3828.1	−249.86	8.7603	−0.1716	0.001408	1188
SF_6	3177.5	−200.57	6.8865	−0.13335	0.0010877	1028
CO_2	2116.8	−136.25	4.7353	−0.092307	0.0007555	668
O_2	1920.4	−135.6	5.2122	−0.10939	0.00093777	568
N_2O	2356.2	−166.38	6.3952	−0.13422	0.0011506	697
DMS	2855.7	−177.63	6.0438	−0.11645	0.00094743	941

[*] Coefficients for fit to $Sc = A + B\,T_c + C\,T_c^2 + D\,T_c^3 + E\,T_c^4$, where T_c is surface temperature in °C

[†] Conservative Temperature should be converted to in situ temperature before using these coefficients

Table 2. Coefficients for fit*,†,‡ of solubility function ϕ_A^0 (mol L^{-1} atm^{-1}).

Gas	a_1	a_2	a_3	a_4	b_1	b_2	b_3
CFC-11	-229.9261	319.6552	119.4471	-1.39165	-0.142382	0.091459	-0.0157274
CFC-12	-218.0971	298.9702	113.8049	-1.39165	-0.143566	0.091015	-0.0153924
SF$_6$	-80.0343	117.232	29.5817	0.0	0.0335183	-0.0373942	0.00774862
CO$_2$	-160.7333	215.4152	89.8920	-1.47759	0.029941	-0.027455	0.0053407
N$_2$O	-165.8806	222.8743	92.0792	-1.48425	-0.056235	0.031619	-0.0048472

* Fit to Eq. (15), where T is in-situ, absolute temperature (K) and S is salinity (practical salinity scale).

† For units of mol m^{-3} atm^{-1}, coefficients should be multiplied by 1000.

‡ The units refer to atm of each gas, not atm of air.

§ When using these coefficients, conservative temperature should be converted to in situ temperature (K) and absolute salinity should be converted to practical salinity.

Table 3. Coefficients for fit of K' and K_0 (both in $\mathrm{mol\,L^{-1}\,atm^{-1}}$).

Gas	a_1	a_2	a_3	b_1	b_2	b_3
				K'		
CFC-11	-134.1536	203.2156	56.2320	-0.144449	0.092952	-0.0159977
CFC-12	-122.3246	182.5306	50.5898	-0.145633	0.092509	-0.0156627
SF_6	-96.5975	139.883	37.8193	0.0310693	-0.0356385	0.00743254
				K_0		
CO_2	-58.0931	90.5069	22.2940	0.027766	-0.025888	0.0050578
N_2O	-62.7062	97.3066	24.1406	-0.058420	0.033193	-0.0051313

[*] Fit to Eq. 24, where T is in-situ, absolute temperature (K) and S is salinity (practical scale).

[†] The final three footnotes of Table 2 also apply here.

Table 4. Output for inert chemistry.

Symbol	Variable name	Units	Shape	Priority	Long name
			Annual means		
CFC-11	cfc11	mol m^{-3}	XYZ	2	Mole Concentration of CFC-11 in Seawater
CFC-12	cfc12	mol m^{-3}	XYZ	1	Mole Concentration of CFC-12 in Seawater
SF$_6$	sf6	mol m^{-3}	XYZ	2	Mole Concentration of SF6 in Seawater
			Monthly means		
$F_{\text{CFC-11}}$	fgcfc11	mol m^{-2} s^{-1}	XY	2	Surface Downward CFC-11 flux
$F_{\text{CFC-12}}$	fgcfc12	mol m^{-2} s^{-1}	XY	1	Surface Downward CFC-12 flux
F_{SF_6}	fgsf6	mol m^{-2} s^{-1}	XY	2	Surface Downward SF6 flux

Table 5. Annual-mean biogeochemical output: Priority 1.

Symbol	Variable name	Units	Shape	Priority	Long name
C_T	dissic	mol m^{-3}	XYZ	1	Dissolved Inorganic Carbon Concentration
C_T^{nat}	dissicnat	mol m^{-3}	XYZ	1	Natural Dissolved Inorganic Carbon Concentration
C_T^{abio}	dissicabio	mol m^{-3}	XYZ	1	Abiotic Dissolved Inorganic Carbon Concentration
$^{14}C_T^{abio}$	dissi14cabio	mol m^{-3}	XYZ	1	Abiotic Dissolved Inorganic 14Carbon Concentration
$^{13}C_T$	dissi13c	mol m^{-3}	XYZ	1	Dissolved Inorganic 13Carbon Concentration
A_T	talk	mol m^{-3}	XYZ	1	Total Alkalinity
A_T^{nat}	talknat	mol m^{-3}	XYZ	1	Natural Total Alkalinity
pH	ph	1	XYZ	1	pH
pH^{nat}	phnat	1	XYZ	1	Natural pH
pH^{abio}	phabio	1	XYZ	1	Abiotic pH
O_2	o2	mol m^{-3}	XYZ	1	Dissolved Oxygen Conentration
NO_3^-	no3	mol m^{-3}	XYZ	1	Dissolved Nitrate Conentration
P_T	po4*	mol m^{-3}	XYZ	1	Total Dissolved Inorganic Phosphorus Concentration
Fe*	dfe†	mol m^{-3}	XYZ	1	Dissolved Iron Concentration
Si_T	si‡	mol m^{-3}	XYZ	1	Total Dissolved Inorganic Silicon Concentration
Chl	chl§	kg m^{-3}	XYZ	1	Mole Concentration of Phytoplankton expressed as Chlorophyll in Seawater
$F_{CO_2^{tot}}$	fgco2	kg m^{-2} s^{-1}	XY	1	Surface Downward Flux of Total CO2
$F_{CO_2^{nat}}$	fgco2nat	kg m^{-2} s^{-1}	XY	1	Surface Downward Flux of Natural CO2
$F_{CO_2^{abio}}$	fgco2abio	kg m^{-2} s^{-1}	XY	1	Surface Downward Flux of Abiotic CO2
$F_{^{14}CO_2^{abio}}$	fg14co2abio	kg m^{-2} s^{-1}	XY	1	Surface Downward Flux of Abiotic 14CO2
$F_{^{14}CO_2}$	fg13co2	kg m^{-2} s^{-1}	XY	1	Surface Downward Flux of 13CO2

* $P_T = H_3PO_4 + H_2PO_4^- + HPO_4^{2-} + PO_4^{3-}$. In seawater most of P_T is in the form of HPO_4^{2-}, while PO_4^{3-} makes up only ∼10% at pH 8.

† dissolved iron in sea water includes both Fe^{2+} and Fe^{3+} ions (but not, e.g. particulate detrital iron)

‡ $Si_T = [Si(OH)_4] + [SiO(OH)_3^-]$, i.e. the sum of silicic acid and silicate

§ sum of chlorophyll from all phytoplankton group concentrations. In most models this is equal to chldiat+chlmisc.

Table 6. Annual-mean biogeochemical output: Priority 2 (concentrations).

Symbol	Variable name	Units	Shape	Priority	Long name
DOC	dissoc	mol m^{-3}	XYZ	2	Dissolved Organic Carbon Concentration
	phyc	mol m^{-3}	XYZ	2	Mole Concentration of Phytoplankton expressed as Carbon in Seawater
	zooc	mol m^{-3}	XYZ	2	Mole Concentration of Zooplankton expressed as Carbon in Seawater
	detoc	mol m^{-3}	XYZ	2	Mole Concentration of Organic Detritus expressed as Carbon in Seawater
$[CaCO_3]_{calc}$	calc	mol m^{-3}	XYZ	2	Mole Concentration of Calcite expressed as Carbon in Seawater
$[CaCO_3]_{arag}$	arag	mol m^{-3}	XYZ	2	Mole Concentration of Aragonite expressed as Carbon in Seawater
$[O_2]_{sat}$	o2sat	mol m^{-3}	XYZ	2	Dissolved Oxygen Concentration at Saturation
$[NH_4^+]$	nh4	mol m^{-3}	XYZ	2	Dissolved Ammonium Concentration
	chldiat[*]	kg m^{-3}	XYZ	2	Diatom Chlorophyll Mass Concentration
	chldiaz[†]	kg m^{-3}	XYZ	2	Mass Concentration of Diazotrophs expressed as Chlorophyll in Seawater
	chlcalc[‡]	kg m^{-3}	XYZ	2	Mass Concentration of Calcareous Phytoplankton expressed as Chlorophyll in Seawater
	chlpico[§]	kg m^{-3}	XYZ	2	Mass Concentration of Picophytoplankton expressed as Chlorophyll in Seawater
	chlmisc[¶]	kg m^{-3}	XYZ	2	Other Phytoplankton Chlorophyll Mass Concentration
	pon	mol m^{-3}	XYZ	2	Particulate Organic Nitrogen Concentration
	pop	mol m^{-3}	XYZ	2	Particulate Organic Phosphorus Concentration
	bfe[1]	mol m^{-3}	XYZ	2	Particulate Biogenic Iron Concentration
	bsi[2]	mol m^{-3}	XYZ	2	Particulate Biogenic Silica Concentration
	phyn	mol m^{-3}	XYZ	2	Phytoplankton Nitrogen Concentration
	phyp	mol m^{-3}	XYZ	2	Phytoplankton Phosphorus Concentration
	phyfe	mol m^{-3}	XYZ	2	Phytoplankton Iron Concentration
	physi	mol m^{-3}	XYZ	2	Phytoplankton Silica Concentration
DMS	dms	mol m^{-3}	XYZ	2	Dimethyl Sulphide Concentration
$[CO_3^{2-}]$	co3	mol m^{-3}	XYZ	2	Carbonate ion Concentration
$[CO_3^{2-}]^{nat}$	co3nat	mol m^{-3}	XYZ	2	Natural Carbonate ion Concentration
$[CO_3^{2-}]^{abio}$	co3abio	mol m^{-3}	XYZ	2	Abiotic Carbonate ion Concentration
$[CO_3^{2-}]_{sat}^{calc}$	co3satcalc	mol m^{-3}	XYZ	2	Carbonate ion Concentration for Seawater in equilibrium with pure Calcite
$[CO_3^{2-}]_{sat}^{arag}$	co3satarag	mol m^{-3}	XYZ	2	Carbonate ion Concentration for Seawater in equilibrium with pure Aragonite

[*] chlorophyll from diatom phytoplankton component concentration alone

[†] chlorophyll concentration from the diazotrophic phytoplankton component alone

[‡] chlorophyll concentration from the calcite-producing phytoplankton component alone

[§] chlorophyll concentration from the picophytoplankton ($<2\ \mu$m) component alone

[¶] chlorophyll from additional phytoplankton component concentrations alone

[1] sum of particulate organic iron component concentrations

[2] sum of particulate silica component concentrations

Table 7. Annual-mean biogeochemical output: Priority 2 (rates).

Variable name	Units	Shape	Priority	Long name
pp	mol m^{-3} s^{-1}	XYZ	2	Primary Carbon Production by Phytoplankton
pnitrate	mol m^{-3} s^{-1}	XYZ	2	Primary Carbon Production by Phytoplankton due to Nitrate Uptake Alone
pbfe	mol m^{-3} s^{-1}	XYZ	2	Biogenic Iron Production
pbsi	mol m^{-3} s^{-1}	XYZ	2	Biogenic Silica Production
pcalc	mol m^{-3} s^{-1}	XYZ	2	Calcite Production
parag	mol m^{-3} s^{-1}	XYZ	2	Aragonite Production
expc	mol m^{-2} s^{-1}	XYZ	2	Sinking Particulate Organic Carbon Flux
expn	mol m^{-2} s^{-1}	XYZ	2	Sinking Particulate Organic Nitrogen Flux
expp	mol m^{-2} s^{-1}	XYZ	2	Sinking Particulate Organic Phosphorus Flux
expfe	mol m^{-2} s^{-1}	XYZ	2	Sinking Particulate Iron Flux
expsi	mol m^{-2} s^{-1}	XYZ	2	Sinking Particulate Silica Flux
expcalc	mol m^{-2} s^{-1}	XYZ	2	Sinking Calcite Flux
exparag	mol m^{-2} s^{-1}	XYZ	2	Sinking Aragonite Flux
remoc	mol m^{-3} s^{-1}	XYZ	2	Remineralization of Organic Carbon
dcalc	mol m^{-3} s^{-1}	XYZ	2	Calcite Dissolution
darag	mol m^{-3} s^{-1}	XYZ	2	Aragonite Dissolution
ppdiat	mol m^{-3} s^{-1}	XYZ	2	Diatom Primary Carbon Production

Table 8. Annual-mean biogeochemical output: Priority 3.

Variable name	Units	Shape	Priority	Long name
bacc	mol m^{-3}	XYZ	3	Bacterial Carbon Concentration
phydiat	mol m^{-3}	XYZ	3	Mole Concentration of Diatoms expressed as Carbon in Seawater
phydiaz	mol m^{-3}	XYZ	3	Mole Concentration of Diazotrophs Expressed as Carbon in Seawater
phycalc	mol m^{-3}	XYZ	3	Mole Concentration of Calcareous Phytoplankton expressed as Carbon in Seawater
phypico[*]	mol m^{-3}	XYZ	3	Mole Concentration of Picophytoplankton expressed as Carbon in Seawater
phymisc[†]	mol m^{-3}	XYZ	3	Mole Concentration of Miscellaneous Phytoplankton expressed as Carbon in Seawater
zmicro[‡]	mol m^{-3}	XYZ	3	Mole Concentration of Microzooplankton expressed as Carbon in Seawater
zmeso[§]	mol m^{-3}	XYZ	3	Mole Concentration of Mesozooplankton expressed as Carbon in Seawater
zmisc[¶]	mol m^{-3}	XYZ	3	Mole Concetration of Other Zooplankton Carbon Concentration
ppdiaz	mol m^{-3} s^{-1}	XYZ	3	Tendency of Mole Concentration of Organic Carbon in Seawater due to NPP by Diazotrophs
ppcalc	mol m^{-3} s^{-1}	XYZ	3	Tendency of Mole Concentration of Organic Carbon in Seawater due to NPP by Calcareous Phytoplankton
pppico	mol m^{-3} s^{-1}	XYZ	3	Tendency of Mole Concentration of Organic Carbon in Seawater due to NPP by Picophytoplankton
ppmisc	mol m^{-3} s^{-1}	XYZ	3	Other Phytoplankton Carbon Production
bddtdic	mol m^{-3} s^{-1}	XYZ	3	Rate of Change of Dissolved Inorganic Carbon due to Biological Activity
bddtdin	mol m^{-3} s^{-1}	XYZ	3	Rate of Change of Nitrogen Nutrient due to Biological Activity
bddtdip	mol m^{-3} s^{-1}	XYZ	3	Rate of Change of Total Dissolved Phosphorus due to Biological Activity
bddtdife	mol m^{-3} s^{-1}	XYZ	3	Rate of Change of Dissolved Inorganic Iron due to Biological Activity
bddtdisi	mol m^{-3} s^{-1}	XYZ	3	Rate of Change of Total Dissolved Inorganic Silicon due to Biological Activity
bddtalk	mol m^{-3} s^{-1}	XYZ	3	Rate of Change of Alkalinity due to Biological Activity
fescav	mol m^{-3} s^{-1}	XYZ	3	Nonbiogenic Iron Scavenging
fediss	mol m^{-3} s^{-1}	XYZ	3	Particle Source of Dissolved Iron
graz	mol m^{-3} s^{-1}	XYZ	3	Total Grazing of Phytoplankton by Zooplankton

[*] carbon concentration from the picophytoplankton (<2 μm) component alone

[†] carbon concentration from additional phytoplankton component alone

[‡] carbon concentration from the microzooplankton (<20 μm) component alone

[§] carbon concentration from mesozooplankton (20–200 μm) component alone

[¶] carbon from additional zooplankton component concentrations alone (e.g. micro, meso). Provides check for model intercomparison since some phytoplankton groups are supersets.

Table 9. Monthly mean biogeochemical output: Priority 1.

Symbol	Variable name	Units	Shape	Priority	Long name
C_T	dissic	mol m^{-3}	XYZ	1	Dissolved Inorganic Carbon Concentration
C_T^{nat}	dissicnat	mol m^{-3}	XYZ	1	Natural Dissolved Inorganic Carbon Concentration
C_T^{abio}	dissicabio	mol m^{-3}	XYZ	1	Abiotic Dissolved Inorganic Carbon Concentration
$^{14}C_T^{abio}$	dissi14cabio	mol m^{-3}	XYZ	1	Abiotic Dissolved Inorganic 14Carbon Concentration
$^{13}C_T$	dissi13c	mol m^{-3}	XYZ	1	Dissolved Inorganic 13Carbon Concentration
A_T	talk	mol m^{-3}	XYZ	1	Total Alkalinity
A_T^{nat}	talknat	mol m^{-3}	XYZ	1	Natural Total Alkalinity
O_2	o2	mol m^{-3}	XYZ	1	Dissolved Oxygen Concentration
NO_3^-	no3	mol m^{-3}	XYZ	1	Dissolved Nitrate Concentration
P_T	po4	mol m^{-3}	XYZ	1	Total Dissolved Inorganic Phosphorus Concentration
Fe	dfe	mol m^{-3}	XYZ	1	Dissolved Iron Concentration
Si_T	si	mol m^{-3}	XYZ	1	Total Dissolved Inorganic Silicon Concentration
Chl	chl	kg m^{-3}	XYZ	1	Total Chlorophyll Mass Concentration
pH	ph	1	XYZ	1	pH
pH^{nat}	phnat	1	XYZ	1	Natural pH
pH^{abio}	phabio	1	XYZ	1	Abiotic pH
	intpp*	mol m^{-2} s^{-1}	XY	1	Primary Organic Carbon Production by All Types of Phytoplankton
	expc100†	mol m^{-2} s^{-1}	XY	1	Downward Flux of Particle Organic Carbon
	expcalc100†	mol m^{-2} s^{-1}	XY	1	Downward Flux of Calcite
	exparag100†	mol m^{-2} s^{-1}	XY	1	Downward Flux of Aragonite
pCO_2	spco2	Pa	XY	1	Surface Aqueous Partial Pressure of CO2
pCO_2^{nat}	spco2nat	Pa	XY	1	Natural Surface Aqueous Partial Pressure of CO2
pCO_2^{abio}	spco2abio	Pa	XY	1	Abiotic Surface Aqueous Partial Pressure of CO2
$F_{CO_2^{tot}}$	fgco2	kg m^{-2} s^{-1}	XY	1	Surface Downward Flux of Total CO2
$F_{CO_2^{nat}}$	fgco2nat	kg m^{-2} s^{-1}	XY	1	Surface Downward Flux of Natural CO2
$F_{CO_2^{abio}}$	fgco2abio	kg m^{-2} s^{-1}	XY	1	Surface Downward Flux of Abiotic CO2
$F_{^{14}CO_2^{abio}}$	fg14co2abio	kg m^{-2} s^{-1}	XY	1	Surface Downward Flux of Abiotic 14CO2
$F_{^{14}CO_2}$	fg13co2	kg m^{-2} s^{-1}	XY	1	Surface Downward Flux of 13CO2
F_{O_2}	fgo2	mol m^{-2} s^{-1}	XY	1	Surface Downward Flux of O2

* Vertically integrated total primary (organic carbon) production by phytoplankton. This should equal the sum of intpdiat+intpphymisc, but those individual components may be unavailable in some models.

† at 100-m depth

Table 10. Monthly mean biogeochemical output: Priority 2.

Symbol	Variable name	Units	Shape	Priority	Long name
DOC	dissoc	mol m^{-3}	XYZ	2	Dissolved Organic Carbon Concentration
	phyc	mol m^{-3}	XYZ	2	Phytoplankton Carbon Concentration
	zooc	mol m^{-3}	XYZ	2	Zooplankton Carbon Concentration
	detoc	mol m^{-3}	XYZ	2	Detrital Organic Carbon Concentration
$[\mathrm{CaCO_3}]_{\mathrm{calc}}$	calc	mol m^{-3}	XYZ	2	Calcite Concentration
$[\mathrm{CaCO_3}]_{\mathrm{arag}}$	arag	mol m^{-3}	XYZ	2	Aragonite Concentration
$[\mathrm{NH_4^+}]$	nh4	mol m^{-3}	XYZ	2	Dissolved Ammonium Concentration
$[\mathrm{CO_3^{2-}}]$	co3	mol m^{-3}	XYZ	2	Carbonate ion Concentration
$[\mathrm{CO_3^{2-}}]^{\mathrm{nat}}$	co3nat	mol m^{-3}	XYZ	2	Natural Carbonate ion Concentration
$[\mathrm{CO_3^{2-}}]^{\mathrm{abio}}$	co3abio	mol m^{-3}	XYZ	2	Abiotic Carbonate ion Concentration
$[\mathrm{CO_3^{2-}}]^{\mathrm{calc}}_{\mathrm{sat}}$	co3satcalc	mol m^{-3}	XYZ	2	Carbonate ion Concentration for Seawater in equilibrium with pure Calcite
$[\mathrm{CO_3^{2-}}]^{\mathrm{arag}}_{\mathrm{sat}}$	co3satarag	mol m^{-3}	XYZ	2	Carbonate ion Concentration for Seawater in equilibrium with pure Aragonite
	limndiat	1	XY	2	Nitrogen limitation of Diatoms
	limirrdiat	1	XY	2	Irradiance limitation of Diatoms
	limfediat	1	XY	2	Iron limitation of Diatoms
	intpnitrate[*]	mol m^{-2} s^{-1}	XY	2	Primary Organic Carbon Production by Phytoplankton Based on Nitrate Uptake Alone
	intppdiat[†]	mol m^{-2} s^{-1}	XY	2	Primary Organic Carbon Production by Diatoms
$\int C_{\mathrm{T}}\,dz$	intdissic[‡]	kg m^{-2}	XY	2	Dissolved Inorganic Carbon Content
$\int DOC\,dz$	intdissoc[§]	kg m^{-2}	XY	2	Dissolved Organic Carbon Content
$\int POC\,dz$	intpoc[¶]	kg m^{-2}	XY	2	Particulate Organic Carbon Content

[*] Vertically integrated primary (organic carbon) production by phytoplankton based on nitrate uptake alone

[†] Vertically integrated primary (organic carbon) production by the diatom phytoplankton component alone

[‡] Vertically integrated C_{T}

[§] Vertically integrated DOC (explicit pools only)

[¶] Vertically integrated POC

Table 11. Monthly mean biogeochemical output: Priority 3 (concentrations)

Variable name	Units	Shape	Priority	Long name
bacc	mol m^{-3}	XYZ	3	Bacterial Carbon Concentration
phydiat	mol m^{-3}	XYZ	3	Mole Concentration of Diatoms expressed as Carbon in Seawater
phydiaz	mol m^{-3}	XYZ	3	Mole Concentration of Diazotrophs Expressed as Carbon in Seawater
phycalc	mol m^{-3}	XYZ	3	Mole Concentration of Calcareous Phytoplankton expressed as Carbon in Seawater
phypico	mol m^{-3}	XYZ	3	Mole Concentration of Picophytoplankton expressed as Carbon in Seawater
phymisc	mol m^{-3}	XYZ	3	Mole Concentration of Miscellaneous Phytoplankton expressed as Carbon in Seawater
zmicro	mol m^{-3}	XYZ	3	Mole Concentration of Microzooplankton expressed as Carbon in Seawater
zmeso	mol m^{-3}	XYZ	3	Mole Concentration of Mesozooplankton expressed as Carbon in Seawater
zmisc	mol m^{-3}	XYZ	3	Other Zooplankton Carbon Concentration
chldiat	kg m^{-3}	XYZ	3	Diatom Chlorophyll Mass Concentration
chldiaz	kg m^{-3}	XYZ	3	Mass Concentration of Diazotrophs expressed as Chlorophyll in Seawater
chlcalc	kg m^{-3}	XYZ	3	Mass Concentration of Calcareous Phytoplankton expressed as Chlorophyll in Seawater
chlpico	kg m^{-3}	XYZ	3	Mass Concentration of Picophytoplankton expressed as Chlorophyll in Seawater
chlmisc	kg m^{-3}	XYZ	3	Other Phytoplankton Chlorophyll Mass Concentration
poc	mol m^{-3}	XYZ	3	Particulate Organic Carbon Concentration
pon	mol m^{-3}	XYZ	3	Particulate Organic Nitrogen Concentration
pop	mol m^{-3}	XYZ	3	Particulate Organic Phosphorus Concentration
bfe	mol m^{-3}	XYZ	3	Particulate Biogenic Iron Concentration
bsi	mol m^{-3}	XYZ	3	Particulate Biogenic Silicon Concentration
phyn	mol m^{-3}	XYZ	3	Phytoplankton Nitrogen Concentration
phyp	mol m^{-3}	XYZ	3	Phytoplankton Phosphorus Concentration
phyfe	mol m^{-3}	XYZ	3	Phytoplankton Iron Concentration
physi	mol m^{-3}	XYZ	3	Phytoplankton Silicon Concentration
dms	mol m^{-3}	XYZ	3	Dimethyl Sulphide Concentration

Table 12. Monthly mean biogeochemical output: Priority 3 (gas exchange, river, burial, N_2 fixation, thresholds)

Symbol	Variable name	Units	Shape	Priority	Long name
$\Delta p\mathrm{CO_2}$	dpco2*	Pa	XY	3	Delta PCO2
$\Delta p\mathrm{CO_2^{nat}}$	dpco2nat*	Pa	XY	3	Natural Delta PCO2
$\Delta p\mathrm{CO_2^{abio}}$	dpco2abio*	Pa	XY	3	Abiotic Delta PCO2
$\Delta p\mathrm{O_2}$	dpo2†	Pa	XY	3	Delta PO2
F_DMS	fgdms	mol m^{-2} s^{-1}	XY	3	Surface Upward Flux of DMS
	icfriver	mol m^{-2} s^{-1}	XY	3	Flux of Inorganic Carbon Into Ocean Surface by Runoff
	fric	mol m^{-2} s^{-1}	XY	3	Downward Inorganic Carbon Flux at Ocean Bottom
	ocfriver	mol m^{-2} s^{-1}	XY	3	Flux of Organic Carbon Into Ocean Surface by Runoff
	froc	mol m^{-2} s^{-1}	XY	3	Downward Organic Carbon Flux at Ocean Bottom
	intpn2	mol m^{-2} s^{-1}	XY	3	Nitrogen Fixation Rate in Ocean
	fsn	mol m^{-2} s^{-1}	XY	3	Surface Downward Net Flux of Nitrogen
	frn	mol m^{-2} s^{-1}	XY	3	Nitrogen Loss to Sediments and through Denitrification
	fsfe	mol m^{-2} s^{-1}	XY	3	Surface Downward Net Flux of Iron
	frfe	mol m^{-2} s^{-1}	XY	3	Iron Loss to Sediments
	o2min	mol m^{-3}	XY	3	Oxygen Minimum Concentration
	zo2min	m	XY	3	Depth of Oxygen Minimum Concentration
CSH	zsatcalc‡	m	XY	3	Calcite Saturation Depth
ASH	zsatarag§	m	XY	3	Aragonite Saturation Depth

*Difference between atmospheric and oceanic partial pressure of CO_2 (positive meaning ocean > atmosphere)

†Difference between atmospheric and oceanic partial pressure of O_2 (positive meaning ocean > atmosphere)

‡Depth of calcite saturation horizon (0 if < surface, "missing" if > bottom, if two, then the shallower)

§Depth of aragonite saturation horizon (0 if < surface, "missing" if > bottom, if two, then the shallower)

Table 13. Monthly mean biogeochemical output: Priority 3 (production and rates of change)

Variable name	Units	Shape	Priority	Long name
expn100*	mol m^{-2} s^{-1}	XY	3	Downward Flux of Particulate Nitrogen
expp100*	mol m^{-2} s^{-1}	XY	3	Downward Flux of Particulate Phosphorus
expfe100*	mol m^{-2} s^{-1}	XY	3	Downward Flux of Particulate Iron
expsi100*	mol m^{-2} s^{-1}	XY	3	Downward Flux of Particulate Silica
fddtdic[†]	mol m^{-2} s^{-1}	XY	3	Rate of Change of Net Dissolved Inorganic Carbon
fddtdin[†,‡]	mol m^{-2} s^{-1}	XY	3	Rate of Change of Net Dissolved Inorganic Nitrogen
fddtdip[†]	mol m^{-2} s^{-1}	XY	3	Rate of Change of Net Dissolved Inorganic Phosphorus
fddtdife[†]	mol m^{-2} s^{-1}	XY	3	Rate of Change of Net Dissolved Inorganic Iron
fddtdisi[†]	mol m^{-2} s^{-1}	XY	3	Rate of Change of Net Dissolved Inorganic Silicon
fddtalk[†]	mol m^{-2} s^{-1}	XY	3	Rate of Change of Total Alkalinity
fbddtdic[†]	mol m^{-2} s^{-1}	XY	3	Rate of Change of Dissolved Inorganic Carbon due to Biological Activity
fbddtdin[†,§]	mol m^{-2} s^{-1}	XY	3	Rate of Change of Dissolved Inorganic Nitrogen due to Biological Activity
fbddtdip[†]	mol m^{-2} s^{-1}	XY	3	Rate of Change of Total Dissolved Inorganic Phosphorus due to Biological Activity
fbddtdife[†]	mol m^{-2} s^{-1}	XY	3	Rate of Change of Dissolved Inorganic Iron due to Biological Activity
fbddtdisi[†]	mol m^{-2} s^{-1}	XY	3	Rate of Change of Total Dissolved Inorganic Silicon due to Biological Activity

* at 100-m depth

[†] integral over upper 100 m only

[‡] Net time rate of change of nitrogen nutrients (e.g. $NO_3^- + NH_4^+$)

[§] Vertical integral of net biological terms in time rate of change of nitrogen nutrients (e.g. $NO_3^- + NH_4^+$)

Table 14. Monthly mean biogeochemical output: Priority 3 (production, grazing, sinking, limitation)

Variable name	Units	Shape	Priority	Long name
pp	mol m^{-3} s^{-1}	XYZ	3	Primary Carbon Production by Phytoplankton
graz	mol m^{-3} s^{-1}	XYZ	3	Total Grazing of Phytoplankton by Zooplankton
expc	mol m^{-2} s^{-1}	XYZ	3	Sinking Particulate Organic Carbon Flux
limndiaz	1	XY	3	Nitrogen limitation of Diazotrophs
limncalc	1	XY	3	Nitrogen limitation of Calcareous Phytoplankton
limnpico	1	XY	3	Nitrogen limitation of Picophytoplankton
limnmisc	1	XY	3	Nitrogen Limitation of Other Phytoplankton
limirrdiaz	1	XY	3	Irradiance limitation of Diazotrophs
limirrcalc	1	XY	3	Irradiance limitation of Calcareous Phytoplankton
limirrpico	1	XY	3	Irradiance limitation of Picophytoplankton
limirrmisc	1	XY	3	Irradiance Limitation of Other Phytoplankton
limfediaz	1	XY	3	Iron limitation of Diazotrophs
limfecalc	1	XY	3	Iron limitation of Calcareous Phytoplankton
limfepico	1	XY	3	Iron limitation of Picophytoplankton
limfemisc	1	XY	3	Iron Limitation of Other Phytoplankton
intppdiaz	mol m^{-2} s^{-1}	XY	3	Net Primary Mole Productivity of Carbon by Diazotrophs
intppcalc	mol m^{-2} s^{-1}	XY	3	Net Primary Mole Productivity of Carbon by Calcareous Phytoplankton
intpppico	mol m^{-2} s^{-1}	XY	3	Net Primary Mole Productivity of Carbon by Picophytoplankton
intppmisc	mol m^{-2} s^{-1}	XY	3	Primary Organic Carbon Production by Other Phytoplankton
intpbn	mol m^{-2} s^{-1}	XY	3	Nitrogen Production
intpbp	mol m^{-2} s^{-1}	XY	3	Phosphorus Production
intpbfe	mol m^{-2} s^{-1}	XY	3	Iron Production
intpbsi	mol m^{-2} s^{-1}	XY	3	Silica Production
intpcalcite	mol m^{-2} s^{-1}	XY	3	Calcite Production
intparag	mol m^{-2} s^{-1}	XY	3	Aragonite Production
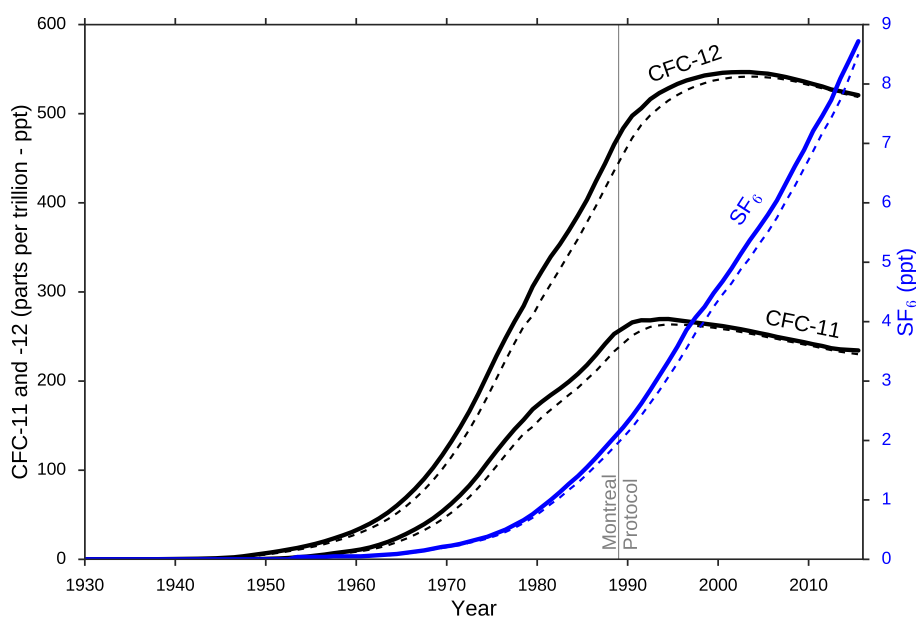
Figure 1. Histories of annual-mean tropospheric mixing ratios of CFC-11, CFC-12, and SF_6 for the northern hemisphere (solid line) and southern hemisphere (dashed line). Mixing ratios are given in parts per trillion (ppt) from mid-year data provided by Bullister (2015). For the OMIP simulations, these inert chemical tracers need not be included until the 4th CORE-II forcing cycle when they will be initialized to zero on 01 January 1936 (at model date 01 January 0237). The vertical grey line indicates the date when the Montreal protocol entered into force.
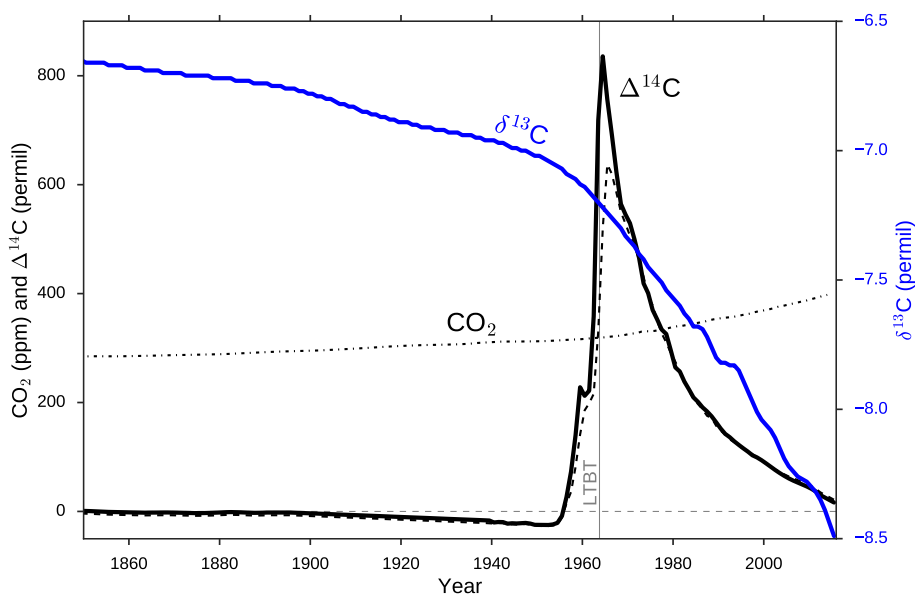
Figure 2. Annual-mean atmospheric histories for global-mean CO_2 (black dash-dot) and $\delta^{13}C$ (blue) compared to hemispheric means of $\Delta^{14}C$ for the north (black solid) and south (black dashes). The CO_2 data are identical to those used for CMIP6 (Meinshausen et al., 2016) and the carbon isotope data are common with C4MIP (Jones et al., 2016). The CO_2 observations are from NOAA (Dlugokencky and Tans, 2016) and Scripps Institution of Oceanography (Keeling et al., 2001), and $\delta^{13}C$ is a compilation of ice-core data (Rubino et al., 2013) and atmospheric measurements at Mauna Loa (Keeling et al., 2001). The $\Delta^{14}C$ data is compiled from Levin et al. (2010) and other sources. Data after 2009 are not used in OMIP Phase 1, but will be used in subsequent phases. Beyond 2009, atmospheric $\Delta^{14}C$ is unpublished data from the University of Heidelberg. Between the beginning of both OMIP simulations on 1 January 1700 and the same date in 1850, the atmospherc concentrations of CO_2, $\delta^{13}C$, and $\Delta^{14}C$ are to be held constant at are 285.375 ppm, -6.8‰ and 0‰, respectively. Also indicated are the preindustrial reference (0 permil) for atmospheric $\Delta^{14}C$ (horizontal grey dashed) and when the Limited Test Ban Treaty (LTBT) went into effect (vertical grey solid).
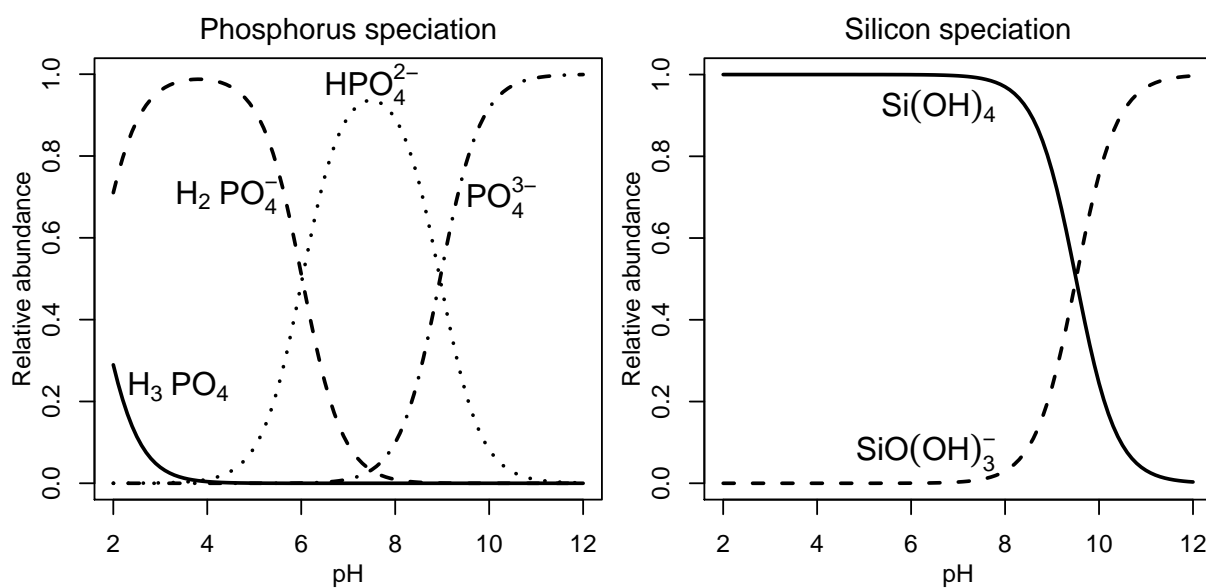
Figure 3. Relative molar abundance of inorganic species of phosphorus (left) and silicon (right) as a function of pH (total scale) in seawater at a temperature of 18°C and salinity of 35.